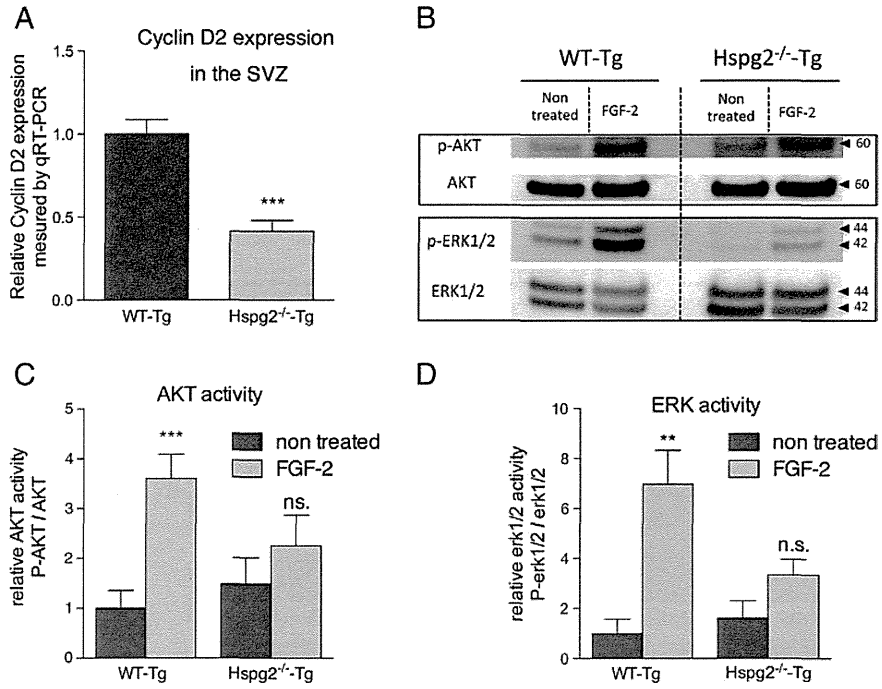

Figure 5 Cyclin D2 expression and FGF-2-induced activation of Akt and Erk1/2 pathways *in vivo*. (A) Bar chart indicates lower cyclin D2 expression in the SVZ of Hspg2$^{-/-}$-Tg compared to WT-Tg mice (n = 4, *** indicates P-value of $P < 0.0001$). (B) Whole SVZ lysates were immunobloted with the indicated antibodies. WT-Tg and Hspg2$^{-/-}$-Tg mice were either not treated or ICV-injected with 0.5 μg of FGF-2 for 30 min prior to sacrifice. (C, D) Bar charts indicate that FGF-2 induced a significant increase of the activation of Akt and Erk1/2 pathways in the WT-tg but not in the Hspg2$^{-/-}$-Tg mice. The data are expressed as means ± SEM (n = 3, *** indicates P-value of P = 0.0007, ** indicates P-value of P = 0.0038; Student's t-test).

in the GCL adjacent to the RMS were reduced by 18% in the absence of perlecan (WT-Tg: 56.12 ± 1.39 BrdU$^+$/NeuN$^+$ cells; Hspg2$^{-/-}$-Tg: 45.76 ± 2.46; Fig. 4E).

We then investigated the nature of the BrdU$^+$ cell population in the olfactory bulb. We found that most BrdU$^+$ cells had begun to express the neuronal marker NeuN (95% of BrdU$^+$ cell co-expressed NeuN). These new neurons (BrdU$^+$/NeuN$^+$) were detected in the GCL (Fig. 4B) and the GL (Fig. 4D). We observed a reduction in the integration of new neurons in the GCL (WT-Tg: 72.15 ± 1.96 BrdU$^+$/NeuN$^+$ cells; Hspg2$^{-/-}$-Tg: 57.73 ± 1.79; Fig. 4C) and the GL (WT-Tg: 7.37 ± 0.40 BrdU$^+$/NeuN$^+$ cells; Hspg2$^{-/-}$-Tg: 5.36 ± 0.34; Fig. 4E) in the perlecan-deficient brain. These data confirmed that the decrease of CD133$^+$ NSCs observed in the perlecan-deficient brain leads to fewer new neurons in the olfactory bulb. Our results show that perlecan is necessary for the maintenance of the CD133$^+$ NSC population, and for neurogenesis.

Perlecan is necessary for FGF-2-induced activation of Akt and Erk1/2 pathways in the subventricular zone

To understand the reason why early events of neurogenesis were impaired in the absence of perlecan, we investigated the expression level of cyclin D2. Cyclin D2 is a protein regulating cell cycle progression in NSPCs. Its expression is necessary for entry into the G_1/S phase of the cell cycle. We found that cyclin D2 expression was significantly reduced in the Hspg2$^{-/-}$-Tg mice (Fig. 5 A). Perlecan is widely recognized as an HSPG modulator of FGF-2 signaling (Aviezer et al., 1994; Rapraeger, 1995). To understand how perlecan regulates FGF-2 activity in the neural stem cell niche, we investigated the activation of the Akt and Erk1/2 pathways in the SVZ after FGF-2 ICV injection. We found that FGF-2 stimulation induced increased phosphorylation of both Akt and Erk1/2 proteins in the WT-Tg mice. However, FGF-2 stimulation failed to activate these two pathways in the absence of perlecan (Fig. 5 B–D). These results indicate that perlecan is necessary for the FGF-2-induced activation of Akt and Erk1/2 pathways *in vivo*.

Neural stem cells express perlecan and can bind FGF-2 *in vitro*

To further investigate the role of FGF-2 on NSCs, we cultivated neurospheres from the cortex of both E16.5 WT-Tg and Hspg2$^{-/-}$-Tg mice. Perlecan was detected in the neurospheres, where its localization was found on the surface of cells that also expressed N-sulfated HS chains (10E4 epitope, Fig. 6A). These cells often coexpressed the stem cell marker CD133 (Fig. 6B). Furthermore, biotinylated FGF-2 was mainly captured by those cells expressing perlecan, 10E4, and CD133. Over 80% of cells that captured FGF-2 also expressed perlecan. However, FGF-2 was not found on the surface of cells expressing chondroitin sulfate chains (Fig. 6C, arrows). This indicates that within the neurosphere CD133$^+$ putative NSCs are surrounded by ECM molecules, such as perlecan and HS chains, and are able to capture FGF-2. To confirm the differentiation potentials of neurospheres, we cultured the primary neurospheres for an additional seven days in the absence of a growth factor.

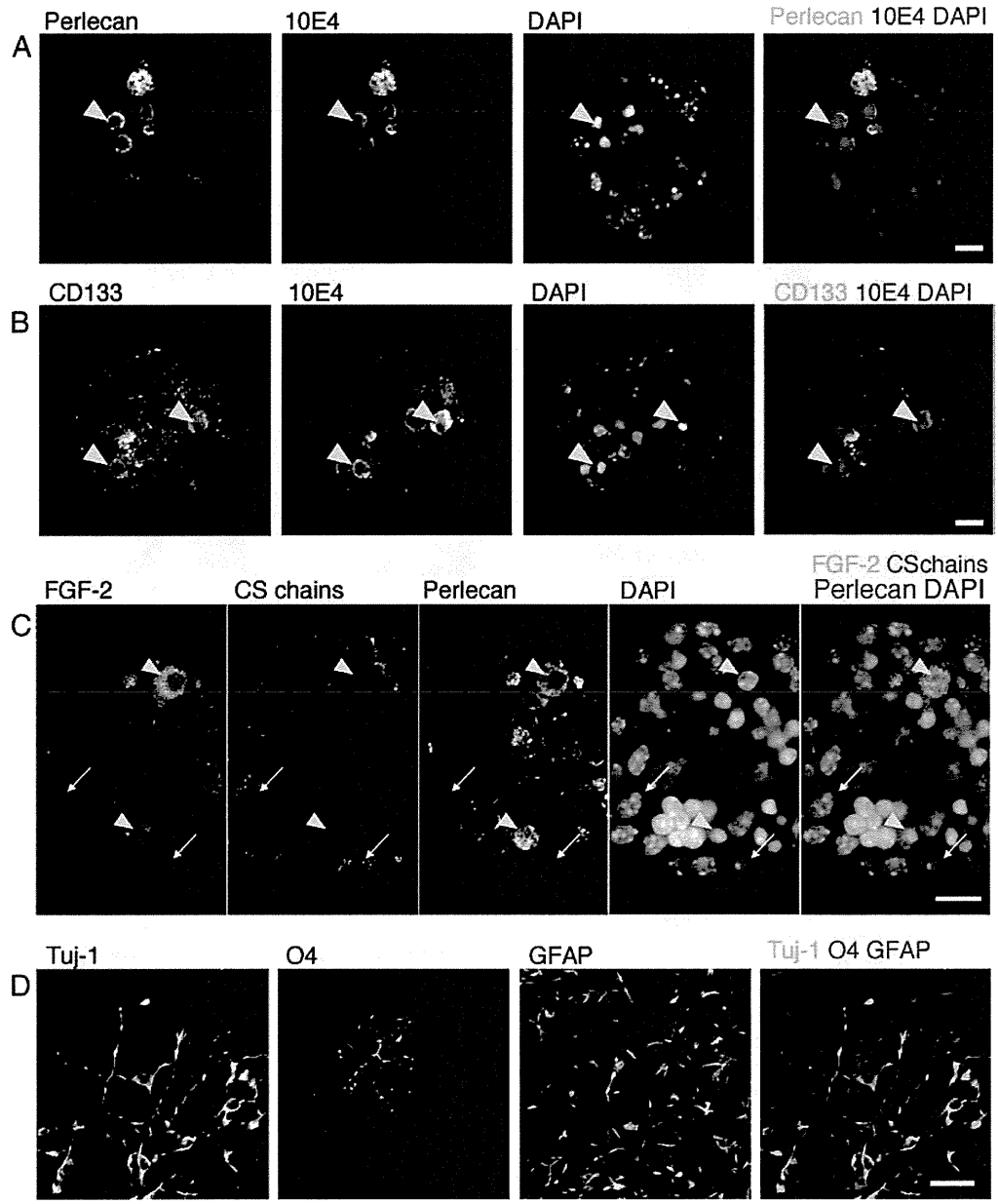

Figure 6 $CD133^+$ NSCs in neurospheres express perlecan and heparan sulfate chains and can capture FGF-2. (A–C) Confocal images of E16.5 WT-Tg neurosphere stained for perlecan, heparan sulfate chains (10E4), CD133, FGF-2, and chondroitin sulfate chains (CS56). Arrowheads point out cells within the neurosphere that co-express perlecan and 10E4 in A, CD133 and 10E4 in B. In C, arrowhead shows that FGF-2 localizes to the surface of cells expressing perlecan but not on the surface of cells that only express chondroitin sulfate chains (arrows). (D) Confocal image of a differentiated neurosphere displaying neurons (stained with Tuj-1), an oligodendrocyte (stained with O4), and astrocytes (stained with GFAP). Scale bar: 10 μm.

We were able to detect oligodendrocytes, neurons, and astrocytes (Fig. 6D).

Perlecan regulates FGF-2 promotion of neurosphere formation

Since FGF-2 activated Akt and Erk1/2 pathways in the SZV of WT-Tg mice but not $Hspg2^{-/-}$-Tg mice, we investigated the effect of FGF-2 on the formation of neurospheres derived from the cortex of both E16.5 WT-Tg and $Hspg2^{-/-}$-Tg mice at different concentrations of FGF-2 (0, 20 and 200 ng/ml). The number of neurospheres from WT-Tg mice increased accordingly due to increases in the FGF-2 concentrations. However, FGF-2 concentrations had no effect on the number of neurospheres from $Hspg2^{-/-}$-Tg (Fig. 7A). We also found that $Hspg2^{-/-}$-Tg neurospheres were significantly smaller (WT-Tg: 83.3 ± 1.58 μm; $Hspg2^{-/-}$-Tg: 52 ± 0.86 μm, Fig. 7B). The basal phosphorylation level of Akt in $Hspg2^{-/-}$-Tg neurospheres was slightly less than that in WT-Tg neurospheres,

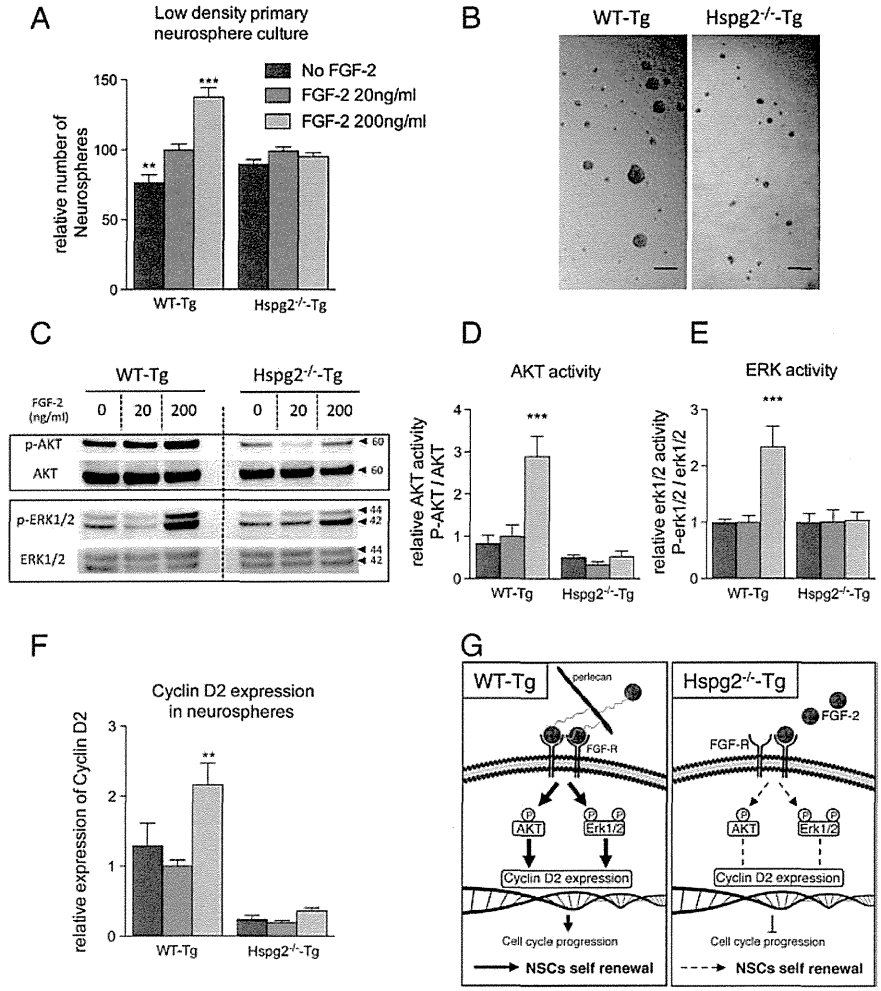

Figure 7 Perlecan is necessary for FGF-2 promotion of neurosphere formation. (A) Low density primary neurosphere culture in the presence of EGF (20 ng/ml) and different concentrations of FGF-2 (0, 20, 200 ng/ml). In the absence of perlecan, FGF-2 fails to promote neurosphere formation. The data are expressed as means ± SEM (n = 6, *** indicates P-value of $P < 0.0001$; ** indicates P-value of $P < 0.001$; one way analysis of variance followed by Bonferroni's multiple comparison test). (B) Bright field images of the primary neurosphere culture after 1 week *in vitro*. The average size of neurospheres from perlecan-deficient brain is significantly smaller (WT-Tg: 83.3 ± 1.58 μm; Hspg2$^{-/-}$-Tg: 52 ± 0.86 μm; $p < 0.0001$). Scale bar: 150 μm. (C) Neurospheres were immunoblotted with indicated antibodies. (D, E) FGF-2 stimulation of Akt and Erk1/2 pathways is impaired in the absence of perlecan. (F) In the absence of perlecan, cyclin D2 expression is significantly reduced and is not responsive to FGF-2 stimulation. (D–F) The data are expressed as means ± SEM (n = 3, *** indicates P-value of $P < 0.001$, ** indicates P-value of $P = 0.0019$. (G) Proposed mechanism of the perlecan function in FGF-2-dependent neurogenesis. In the presence of perlecan, FGF-2 activates Akt and Erk1/2 pathways and increases cyclin D2 expression leading to the progression of the cell cycle thus allowing NSCs self renewal and neurogenesis. In absence of perlecan, this series of event is greatly impaired.

whereas the basal phosphorylation level of Erk1/2 was similar between Hspg2$^{-/-}$-Tg and WT-Tg neurospheres (Fig. 7C–E). The addition of FGF-2 at a high concentration (200 ng/ml) to the culture induced a significant increase in the phosphorylation levels of both Akt and Erk1/2 in the WT-Tg mice, whereas this FGF effect was much less in Hspg2$^{-/-}$-Tg mice (Fig. 7C–E). Furthermore, the expression of cyclin D2 was less in Hspg2$^{-/-}$-Tg neurospheres than the level in WT-Tg neurospheres (Fig. 7F). The high concentration of FGF-2 also significantly increased cyclin D2 expression in WT-Tg neurospheres. In Hspg2$^{-/-}$-Tg neurospheres, the level of induction of the cyclin D2 expression by FGF was less than that in WT-Tg neurospheres (Fig. 7 F). Hence, we propose in Fig. 7 G that perlecan is necessary for FGF-2 to activate the Akt and Erk1/2 pathways, thus leading to cyclin D2 expression, cell cycle progression, and ultimately NSCs self-renewal and proliferation. Taken together, our results strongly suggest that perlecan affects FGF-2 dependent maintenance of NSCs.

Discussion

Extracellular matrix in the neurogenic niche of Hspg2$^{-/-}$-Tg mice

We previously reported some disparities in the composition of ECM components in fractones and nearby capillaries when

these were compared with blood vessels outside the SVZ. Laminin α1 (Lama1) is present in large (>25 μm of diameter) arteries and arterioles, while other basement membrane molecules, such as laminin β1 (Lamb1), perlecan, collagen IV, and nidogen, are present in all blood vessels and in fractones (Mercier et al., 2002). We also reported that 10E4 antibody staining for heparan sulfate chains was primarily observed in fractones and in SVZ blood vessels (Kerever et al., 2007; Mercier and Arikawa-Hirasawa, 2012; Douet et al., 2013). In the present study, we showed that agrin was expressed in fractones and in blood vessel basement membranes (as we previously reported for perlecan), but that collagen 18 was only expressed in blood vessels from adjacent neural nuclei. We found that all three different antibodies to HS chains stained fractones and SVZ blood vessels, and these showed no obvious changes in their expression patterns in the absence of perlecan. It is unlikely that collagen 18 compensates for perlecan loss to maintain those HS chains because it was absent in the neurogenic niche. Agrin most likely accounts for this staining, since it is a proteoglycan that bears heparan sulfate chains. Therefore, our data suggest that HS chains and/or the protein core of perlecan are involved in neurogenesis because the absence of perlecan greatly impaired neurogenesis.

Neural stem cell maintenance

A specific marker for the identification of NSCs is still lacking because most recognized markers are also expressed by other cell types. Therefore, we used a combination of CD133 and GFAP, two markers present in NSCs. GFAP and CD133 can be found in SVZ astrocytes and in ependymocytes, respectively. The use of both markers allowed us to characterize a specific cell population. Type B cells frequently penetrate the ependymal layer to contact the ventricle (Mirzadeh et al., 2008; Shen et al., 2008). Indeed, we observed that $CD133^+GFAP^+$ cells often extended processes contacting the ventricle where CD133 was absent in ependymal cells (Fig. 2B). One possible explanation for the decrease in $CD133^+$ NSCs in the perlecan-deficient brain may be that perlecan serves as a survival factor. Staining for an apoptosis marker, single-stranded DNA (SSDNA), showed negligible cell death in the SVZ of WT-Tg and $Hspg2^{-/-}$-Tg mice (Supplemental Fig. 4), similar to that in the SVZ of wild type mice as reported (Shen et al., 2008). Notably, some $CD133^-$ cells also share NSC properties (Sun et al., 2009), and CD133 is expressed in type B1 cells, a subpopulation of type B cells that function as NSCs (Mirzadeh et al., 2008). Both NSC populations ($CD133^+GFAP^+$ and $CD133^-GFAP^+$) may therefore coexist in the adult SVZ. However, the necessity of CD133 expression for differentiation is unknown. Sun et al. reported that the $CD133^-$ NSC population is mainly in the G_0/G_1 phase, while the $CD133^+$ NSC population is evenly split between G_0/G_1 and G_2/M. Moreover, when cultured, the progeny of this $CD133^-$ NSC population reacquired CD133. This suggests that a transition from a quiescent $CD133^-$ NSC into a $CD133^+$ NSC is possible in vitro.

Cyclin D2 is a G_1 active cyclin that is necessary for the progression of the cell cycle. The lack of functional cyclin D2 leads to a critically impaired adult neurogenesis (Kowalczyk, 2004). Here we observed that in the absence of perlecan, cyclin D2 expression was significantly reduced both *in vivo* and *in vitro*. These results further suggest that perlecan is necessary for the cyclin D2-mediated progression of the NSC cell cycle.

We observed a reduction in the numbers of type C and type A cells in the SVZ, but this reduction was proportional to the decrease in CD133 + GFAP + NSCs in the absence of perlecan. If perlecan was involved in the differentiation process into type A cells, we would have expected a stronger decrease in the population of new neuroblasts in the SVZ. Our results suggest that perlecan was not necessary to amplify type C cells or to differentiate into type A cells, but that it was necessary to maintain the population of NSCs.

We found that the decrease in the size of the RMS in $Hspg2^{-/-}$-Tg mice was equivalent to the decreased number of type A cells exiting the SVZ. Therefore, perlecan may not be necessary for the migration of neuroblasts. Once neuroblasts arrive in the olfactory bulb, the majority of them start to differentiate into mature neurons in the granule cell layer. Others migrate further to the glomerular layer, where they differentiate into periglomerular neurons. We observed a decrease in the integration of new neurons into the olfactory bulb in both the granule cell layer and the glomerular layer in $Hspg2^{-/-}$-Tg mice. These results are consistent with the decrease in numbers of $CD133^+GFAP^+$ NSCs, which resulted in a decrease in new neurons integrating into the olfactory bulb.

Perlecan is involved in angiogenesis through the binding and modulation of growth factor activity (Aviezer et al., 1994; Ishijima et al., 2012). Removal of perlecan HS chains causes impaired tumor angiogenesis and tumor growth (Zhou, 2004). $CD133^+$ cancer stem cells have been identified as a critical cell population for resistance to chemotherapy (Liu et al., 2006). Our findings in the present study that perlecan is critical for $CD133^+$ NSCs, open the question of whether perlecan plays a role in the maintenance of $CD133^+$ cancer stem cells.

FGF-2 stimulation of neurogenesis is impaired in the absence of perlecan

In this study, we showed that the ability to form neurospheres in response to FGF-2 stimulation was less effective in the absence of perlecan. Furthermore, the activation of Akt and Erk1/2, two major downstream signaling pathway of FGF-2, was critically impaired both *in vivo* and *in vitro* in the absence of perlecan. Furthermore, cyclin D2 expression which has been shown to be positively regulated by the activation of the Akt and Erk pathways (Dey et al., 2000; Fatrai et al., 2006), also failed to increase following FGF-2 stimulation in neurospheres derived from perlecan-deficient mice. Hence, we proposed that the absence of perlecan critically affects FGF-2 signaling, which results in reduced cyclin D2 expression and eventually a significant decrease in the NSC self-renewal and neurogenesis.

Chondroitin sulfate (CS) glycosaminoglycans have also been suggested to play a role in FGF-2 signaling (Filla et al., 1998; Hagihara et al., 2000; Sirko et al., 2010). We previously reported that fractones and SVZ blood vessels specifically capture FGF-2 from the extracellular milieu (Kerever et al., 2007). However, we did not detect CS chains in the fractones and in the SVZ blood vessels of either the WT-Tg or the $Hspg2^{-/-}$-Tg mice. Furthermore, FGF-2 localization was

correlated with cells expressing perlecan but not with cells expressing CS chains in neurospheres. These results suggest that perlecan is the major proteoglycans responsible for the management of heparin-binding growth factors, such as FGF-2, in the neurogenic niche.

An extracellular matrix niche for neurogenesis

Previous studies have introduced the concept of the vascular niche for neurogenesis in the SVZ (Shen et al., 2008; Tavazoie et al., 2008; Kojima et al., 2010). At the vascular basement membrane interface, the fate of NSCs is influenced by signals diffusing from endothelial cells (Shen et al., 2008), and also by signals traveling through the blood–brain barrier (Tavazoie et al., 2008). The contact between $\alpha 6\beta 1$ integrins of NSCs and laminin in the blood vessel basement membrane is crucial for the positioning and proliferation of NSCs (Shen et al., 2008; Tavazoie et al., 2008). In addition, fractones have been implicated as crucial niche components that are tightly associated with NSCs (Mercier et al., 2002, 2003; Kerever et al., 2007; Mercier and Arikawa-Hirasawa, 2012; Douet et al., 2013). Growth factors, such as FGF-2 and BMP-7, in the cerebrospinal fluid may penetrate the ependymal wall through the interstitial cleft, a structure identified by MW. Brightman (1965; 2002) and can be captured by fractones (Kerever et al., 2007; Douet et al., 2012) to regulate adult neurogenesis (Douet et al., 2012; Douet et al., 2013).Since both fractones and SVZ blood vessels contain perlecan, it is likely to be involved in modulating signaling from the blood vessels and from the cerebrospinal fluid. We showed that FGF-2-promoted neurogenesis is impaired in the absence of perlecan. Taken together, these results strongly suggest that perlecan regulates neurogenesis by modulating the growth factor activity in the neurogenic niche. Our study revealed that perlecan is a critical extracellular matrix component of the neurogenic niche with multiple functions in development and in maintaining tissue.

Supplementary data to this article can be found online at http://dx.doi.org/10.1016/j.scr.2013.12.009.

Acknowledgments

This work was supported by grants from MEXT-Supported Program for the Strategic Research Foundation at Private Universities (2011–2015) and the Ministry of Education, Culture, Sports Science, and Technology of Japan (17082008 and 2230023 to E. A-H.) and the Intramural Program of the NIDCR, National Institutes of Health (Y.Y.). Bernard Zalc has received funding from the program "Investissements d'avenir" ANR-10-IAIHU-06.

References

Altman, J., 1963. Autoradiographic investigation of cell proliferation in the brains of rats and cats. Anat. Rec. 145, 573–591.

Altman, J., 1969. Autoradiographic and histological studies of postnatal neurogenesis. IV. Cell proliferation and migration in the anterior forebrain, with special reference to persisting neurogenesis in the olfactory bulb. J. Comp. Neurol. 137, 433–457.

Arikawa-Hirasawa, E., Koga, R., Tsukahara, T., Nonaka, I., Mitsudome, A., Goto, K., Beggs, A.H., Arahata, K., 1995. A severe muscular dystrophy patient with an internally deleted very short (110 kD) dystrophin: presence of the binding site for dystrophin-associated glycoprotein (DAG) may not be enough for physiological function of dystrophin. Neuromuscul. Disord. 5, 429–438.

Arikawa-Hirasawa, E., Watanabe, H., Takami, H., Hassell, J.R., Yamada, Y., 1999. Perlecan is essential for cartilage and cephalic development. Nat. Genet. 23, 354–358.

Arikawa-Hirasawa, E., Wilcox, W.R., Le, A.H., Silverman, N., Govindraj, P., Hassell, J.R., Yamada, Y., 2001. Dyssegmental dysplasia, Silverman-Handmaker type, is caused by functional null mutations of the perlecan gene. Nat. Genet. 27, 431–434.

Arikawa-Hirasawa, E., Le, A.H., Nishino, I., Nonaka, I., Ho, N.C., Francomano, C.A., Govindraj, P., Hassell, J.R., Devaney, J.M., Spranger, J., et al., 2002a. Structural and functional mutations of the perlecan gene cause Schwartz-Jampel syndrome, with myotonic myopathy and chondrodysplasia. Am. J. Hum. Genet. 70, 1368–1375.

Arikawa-Hirasawa, E., Rossi, S.G., Rotundo, R.L., Yamada, Y., 2002b. Absence of acetylcholinesterase at the neuromuscular junctions of perlecan-null mice. Nat. Neurosci. 5, 119–123.

Aviezer, D., Hecht, D., Safran, M., Eisinger, M., David, G., Yayon, A., 1994. Perlecan, basal lamina proteoglycan, promotes basic fibroblast growth factor-receptor binding, mitogenesis, and angiogenesis. Cell 79, 1005–1013.

Brightman, M.W., 1965. The distribution within the brain of ferritin injected into cerebrospinal fluid compartments. I. Ependymal distribution. J. Cell Biol. 26, 99–123.

Brightman, M.W., 2002. The brain's interstitial clefts and their glial walls. J. Neurocytol. 31, 595–603.

Chan, J.A., Balasubramanian, S., Witt, R.M., Nazemi, K.J., Choi, Y., Pazyra-Murphy, M.F., Walsh, C.O., Thompson, M., Segal, R.A., 2009. Proteoglycan interactions with Sonic Hedgehog specify mitogenic responses. Nat. Neurosci. 12, 409–417.

Corti, S., Nizzardo, M., Nardini, M., Donadoni, C., Locatelli, F., Papadimitriou, D., Salani, S., Del Bo, R., Ghezzi, S., Strazzer, S., et al., 2007. Isolation and characterization of murine neural stem/progenitor cells based on Prominin-1 expression. Exp. Neurol. 205, 547–562.

Costell, M., Gustafsson, E., Aszódi, A., Mörgelin, M., Bloch, W., Hunziker, E., Addicks, K., Timpl, R., Fässler, R., 1999. Perlecan maintains the integrity of cartilage and some basement membranes. J. Cell Biol. 147, 1109–1122.

Dey, A., She, H., Kim, L., Boruch, A., Guris, D.L., Carlberg, K., Sebti, S.M., Woodley, D.T., Imamoto, A., Li, W., 2000. Colony-stimulating factor-1 receptor utilizes multiple signaling pathways to induce cyclin D2 expression. Mol. Biol. Cell 11, 3835–3848.

Doetsch, F., García-Verdugo, J.M., Alvarez-Buylla, A., 1997. Cellular composition and three-dimensional organization of the subventricular germinal zone in the adult mammalian brain. J. Neurosci. 17, 5046–5061.

Doetsch, F., Caillé, I., Lim, D.A., García-Verdugo, J.M., Alvarez-Buylla, A., 1999. Subventricular zone astrocytes are neural stem cells in the adult mammalian brain. Cell 97, 703–716.

Douet, V., Arikawa-Hirasawa, E., Mercier, F., 2012. Fractone-heparan sulfates mediate BMP-7 inhibition of cell proliferation in the adult subventricular zone. Neurosci. Let. 528 (2), 120–125.

Douet, V., Kerever, A., Arikawa-Hirasawa, E., Mercier, F., 2013. Fractone-heparan sulphates mediate FGF-2 stimulation of cell proliferation in the adult subventricular zone. Cell Prolif. 46, 137–145.

Eriksson, P.S., Perfilieva, E., Björk-Eriksson, T., Alborn, A.M., Nordborg, C., Peterson, D.A., Gage, F.H., 1998. Neurogenesis in the adult human hippocampus. Nat. Med. 4, 1313–1317.

Fatrai, S., Elghazi, L., Balcazar, N., Cras-Méneur, C., Krits, I., Kiyokawa, H., Bernal-Mizrachi, E., 2006. Akt induces beta-cell proliferation by regulating cyclin D1, cyclin D2, and p21 levels and cyclin-dependent kinase-4 activity. Diabetes 55, 318–325.

Filla, M.S., Dam, P., Rapraeger, A.C., 1998. The cell surface proteoglycan syndecan-1 mediates fibroblast growth factor-2 binding and activity. J. Cell. Physiol. 174, 310–321.

Fischer, J., Beckervordersandforth, R., Tripathi, P., Steiner-Mezzadri, A., Ninkovic, J., Götz, M., 2011. Prospective isolation of adult neural stem cells from the mouse subependymal zone. Nat. Protoc. 6, 1981–1989.

Girós, A., Morante, J., Gil-Sanz, C., Fairén, A., Costell, M., 2007. Perlecan controls neurogenesis in the developing telencephalon. BMC Dev. Biol. 7, 29.

Hagihara, K., Watanabe, K., Chun, J., Yamaguchi, Y., 2000. Glypican-4 is an FGF2-binding heparan sulfate proteoglycan expressed in neural precursor cells. Dev. Dyn. 219, 353–367.

Ishijima, M., Suzuki, N., Hozumi, K., Matsunobu, T., Kosaki, K., Kaneko, H., Hassell, J.R., Arikawa-Hirasawa, E., Yamada, Y., 2012. Perlecan modulates VEGF signaling and is essential for vascularization in endochondral bone formation. Matrix Biol. 31, 234–245.

Kerever, A., Schnack, J., Vellinga, D., Ichikawa, N., Moon, C., Arikawa-Hirasawa, E., Efird, J.T., Mercier, F., 2007. Novel extracellular matrix structures in the neural stem cell niche capture the neurogenic factor fibroblast growth factor 2 from the extracellular milieu. Stem Cells 25, 2146–2157.

Kojima, T., Hirota, Y., Ema, M., Takahashi, S., Miyoshi, I., Okano, H., Sawamoto, K., 2010. Subventricular zone-derived neural progenitor cells migrate along a blood vessel scaffold toward the post-stroke striatum. Stem Cells 28 (3), 545–554.

Kowalczyk, A., 2004. The critical role of cyclin D2 in adult neurogenesis. J. Cell Biol. 167, 209–213.

Liu, G., Yuan, X., Zeng, Z., Tunici, P., Ng, H., Abdulkadir, I.R., Lu, L., Irvin, D., Black, K.L., Yu, J.S., 2006. Analysis of gene expression and chemoresistance of CD133+ cancer stem cells in glioblastoma. Mol. Cancer 5, 67.

Lois, C., Alvarez-Buylla, A., 1994. Long-distance neuronal migration in the adult mammalian brain. Science 264, 1145–1148.

Maric, D., Fiorio Pla, A., Chang, Y.H., Barker, J.L., 2007. Self-renewing and differentiating properties of cortical neural stem cells are selectively regulated by basic fibroblast growth factor (FGF) signaling via specific FGF receptors. J. Neurosci. 27, 1836–1852.

Mercier, F., Arikawa-Hirasawa, E., 2012. Heparan sulfate niche for cell proliferation in the adult brain. Neurosci. Lett. 1–6.

Mercier, F., Kitasako, J.T., Hatton, G.I., 2002. Anatomy of the brain neurogenic zones revisited: fractones and the fibroblast/macrophage network. J. Comp. Neurol. 451, 170–188.

Mercier, F., Kitasako, J.T., Hatton, G.I., 2003. Fractones and other basal laminae in the hypothalamus. J. Comp. Neurol. 455, 324–340.

Mirzadeh, Z., Merkle, F.T., Soriano-Navarro, M., Garcia-Verdugo, J.M., Alvarez-Buylla, A., 2008. Neural stem cells confer unique pinwheel architecture to the ventricular surface in neurogenic regions of the adult brain. Cell Stem Cell 3, 265–278.

Palmer, T.D., Ray, J., Gage, F.H., 1995. FGF-2-responsive neuronal progenitors reside in proliferative and quiescent regions of the adult rodent brain. Mol. Cell. Neurosci. 6, 474–486.

Palmer, T.D., Willhoite, A.R., Gage, F.H., 2000. Vascular niche for adult hippocampal neurogenesis. J. Comp. Neurol. 425, 479–494.

Pastrana, E., Cheng, L.C., Doetsch, F., 2009. Simultaneous prospective purification of adult subventricular zone neural stem cells and their progeny. Proc. Natl. Acad. Sci. 106 (15), 6387–6392.

Petreanu, L., Alvarez-Buylla, A., 2002. Maturation and death of adult-born olfactory bulb granule neurons: role of olfaction. J. Neurosci. 22, 6106–6113.

Raballo, R., Rhee, J., Lyn-Cook, R., Leckman, J.F., Schwartz, M.L., Vaccarino, F.M., 2000. Basic fibroblast growth factor (Fgf2) is necessary for cell proliferation and neurogenesis in the developing cerebral cortex. J. Neurosci. 20, 5012–5023.

Rapraeger, A.C., 1995. In the clutches of proteoglycans: how does heparan sulfate regulate FGF binding? Chem. Biol. 2, 645–649.

Seki, T., Arai, Y., 1993. Highly polysialylated neural cell adhesion molecule (NCAM-H) is expressed by newly generated granule cells in the dentate gyrus of the adult rat. J. Neurosci. 13, 2351–2358.

Shen, Q., Wang, Y., Kokovay, E., Lin, G., Chuang, S.-M., Goderie, S.K., Roysam, B., Temple, S., 2008. Adult SVZ stem cells lie in a vascular niche: a quantitative analysis of niche cell–cell interactions. Cell Stem Cell 3, 289–300.

Sirko, S., von Holst, A., Weber, A., Wizenmann, A., Theocharidis, U., Götz, M., Faissner, A., 2010. Chondroitin sulfates are required for fibroblast growth factor-2-dependent proliferation and maintenance in neural stem cells and for epidermal growth factor-dependent migration of their progeny. Stem Cells 28, 775–787.

Sun, Y., Kong, W., Falk, A., Hu, J., Zhou, L., Pollard, S., Smith, A., 2009. CD133 (prominin) negative human neural stem cells are clonogenic and tripotent. PLoS One 4, e5498.

Tavazoie, M., Van der Veken, L., Silva-Vargas, V., Louissaint, M., Colonna, L., Zaidi, B., Garcia-Verdugo, J.M., Doetsch, F., 2008. A specialized vascular niche for adult neural stem cells. Cell Stem Cell 3, 279–288.

Tsumaki, N., Tanaka, K., Arikawa-Hirasawa, E., Nakase, T., Kimura, T., Thomas, J.T., Ochi, T., Luyten, F.P., Yamada, Y., 1999. Role of CDMP-1 in skeletal morphogenesis: promotion of mesenchymal cell recruitment and chondrocyte differentiation. J. Cell Biol. 144, 161–173.

Uchida, N., Buck, D.W., He, D., Reitsma, M.J., Masek, M., Phan, T.V., Tsukamoto, A.S., Gage, F.H., Weissman, I.L., 2000. Direct isolation of human central nervous system stem cells. Proc. Natl. Acad. Sci. U. S. A. 97, 14720–14725.

Voigt, A., Pflanz, R., Schäfer, U., Jäckle, H., 2002. Perlecan participates in proliferation activation of quiescent Drosophila neuroblasts. Dev. Dyn. 224, 403–412.

Winner, B., Cooper-Kuhn, C.M., Aigner, R., Winkler, J., Kuhn, H.G., 2002. Long-term survival and cell death of newly generated neurons in the adult rat olfactory bulb. Eur. J. Neurosci. 16, 1681–1689.

Xu, Z., Ichikawa, N., Kosaki, K., Yamada, Y., Sasaki, T., Sakai, L.Y., Kurosawa, H., Hattori, N., Arikawa-Hirasawa, E., 2010. Perlecan deficiency causes muscle hypertrophy, a decrease in myostatin expression, and changes in muscle fiber composition. Matrix Biol. 29, 461–470.

Yayon, A., Klagsbrun, M., Esko, J.D., Leder, P., Ornitz, D.M., 1991. Cell surface, heparin-like molecules are required for binding of basic fibroblast growth factor to its high affinity receptor. Cell 64, 841–848.

Zhou, Z., 2004. Impaired angiogenesis, delayed wound healing and retarded tumor growth in perlecan heparan sulfate-deficient mice. Cancer Res. 64, 4699–4702.

Perlecan-Deficient Mutation Impairs Corneal Epithelial Structure

Takenori Inomata,[1,2] *Nobuyuki, Ebihara,*[1] *Toshinari Funaki,*[1] *Akira Matsuda,*[1] *Yasuo Watanabe,*[1] *Liang Ning,*[2] *Zhuo Xu,*[2] *Akira Murakami,*[1] *and Eri Arikawa-Hirasawa*[2,3]

Purpose. To elucidate the role of perlecan (Hspg2), a large multidomain heparan sulfate proteoglycan expressed in the basement membrane, in the structure of the corneal epithelium.

Methods. A previously developed perlecan-deficient (*Hspg2*$^{-/-}$-Tg) mouse model was used. Histologic analysis of their corneas was performed by light and transmission electron microscopy. The localization of perlecan in the corneas of wild-type (WT) mice and *Hspg2*$^{-/-}$-Tg mice was examined by immunohistochemistry. The effects of perlecan deficiency on corneal epithelial structure was analyzed with respect to the expression of corneal epithelial proliferation and differentiation markers, such as Ki67, cytokeratin12 (K12), connexin43 (Cx43), Notch1, and Pax6 by immunohistochemistry and real-time polymerase chain reaction (PCR).

Results. The *Hspg2*$^{-/-}$-Tg mice had microphthalmos and a thinner corneal epithelium compared with that of the WT mice. Perlecan was localized in the corneal epithelial basement membrane in the WT mice, but not in the *Hspg2*$^{-/-}$-Tg mice. The *Hspg2*$^{-/-}$-Tg corneal epithelium exhibited thinner wing cell layers and a decreased number of Ki67-positive cells, but no dead cells, compared with the WT corneal epithelium. Immunohistochemistry and real-time PCR analysis revealed a significantly decreased expression of corneal epithelial differentiation markers such as K12, Cx43, Notch1, and Pax6 in *Hspg2*$^{-/-}$-Tg mice, compared with those of the WT mice.

Conclusions. The findings of this study highlight a strong correlation between the presence of perlecan in the basement membrane and the structure of corneal epithelium and that the perlecan-deficient mutation impairs corneal epithelial structure. (*Invest Ophthalmol Vis Sci.* 2012;53:1277–1284) DOI:10.1167/iovs.11-8742

The surface of a mammalian cornea is composed of a nonkeratinized, self-renewing, pluristratified epithelium of ectodermal origin. The corneal epithelium consists of basal, wing, and superficial cells that are separated from the stroma by the basement membrane (BM). Corneal epithelial cells exhibit a dynamic homeostasis, turning over approximately every 7 to 10 days. Many cellular processes, such as proliferation, apoptosis, differentiation, migration, adhesion, and stratification, are essential for the structure of corneal epithelium.

Perlecan (Hspg2) is a large (>400 kDa), multidomain heparan sulfate proteoglycan (Hspg) expressed in BM.[1–6] The protein core consists of five domains that share homology with other molecules involved in nutrient metabolism, cell proliferation, and adhesion, including laminin, the low-density lipoprotein (LDL) receptor, epithelial growth factor (EGF), and the neural cell adhesion molecule (N-CAM).[1–3] Within the protein core there are numerous sites for O-linked glycosylation, as well as four potential sites for heparan sulfate (HS)/chondroitin sulfate (CS) chain attachment. These chains, which are usually HS, have been shown to be involved in many interactions, including those associated with growth factors, extracellular matrix (ECM) molecules, and neuromuscular junction proteins.[1–3,7] Perlecan regulates cells through a basic mechanism involving the binding of various proteins via the protein core and/or the glycosaminoglycan chains. In vertebrates, perlecan functions in a diverse range of developmental and biological processes, from the development of cartilage to the regulation of wound healing.[8–13] Recent reports from other groups also emphasized a key role for perlecan in regulating cell proliferation and cell survival in different tissues. For example, it has been reported that perlecan HS deficiency induces apoptosis of lens epithelial cells.[14] Sher et al.[15] found that perlecan regulates both the survival and terminal differentiation steps of keratinocytes and that it is critical for the formation of normal epidermis.

In the cornea, perlecan is expressed in the BM of the corneal epithelium.[16] However, the functions or roles of perlecan in the cornea have yet to be well investigated. Therefore, in the present study, the role of perlecan in the structure of corneal epithelium was investigated by use of perlecan-deficient (*Hspg2*$^{-/-}$-Tg) mice. By genetically disrupting perlecan expression in the BM of corneal epithelium, the results of this study revealed that perlecan is essential in the structure of corneal epithelium. To the best of our knowledge, this study is the first to demonstrate the involvement of perlecan in the structure of the corneal epithelium.

Materials and Methods

Animal Experiments

Some perlecan-deficient (*Hspg2*$^{-/-}$) mice die around embryonic day (E)10 due to defects in the myocardial basement membranes, and the mice that survive this stage die perinatally of premature cartilage development.[12,17] In a previous study, a perlecan transgenic mouse line (Tg, *Col2a1-Hspg2*$^{Tg/-}$) that expresses recombinant perlecan in cartilage was created by use of a cartilage-specific *Col2a1* promoter/enhancer to reverse the cartilage abnormalities of *Hspg2*$^{-/-}$ mice.[13] Perinatal lethality–rescued mice (*Hspg2*$^{-/-}$-Tg, *Hspg2*$^{-/-}$; *Col2a1-*

From the Departments of [1]Ophthalmology and [3]Neurology and the [2]Research Institute for Disease of Old Age, Juntendo University School of Medicine, Tokyo, Japan.

Submitted for publication October 5, 2011; revised November 16, 2011, and January 6, 2012; accepted January 10, 2012.

Disclosure: **T. Inomata**, None; **N. Ebihara** , None; **T. Funaki** , None; **A. Matsuda**, None; **Y. Watanabe**, None; **L. Ning**, None; **Z. Xu**, None; **A. Murakami**, None; **E. Arikawa-Hirasawa**, None

Corresponding author: Nobuyuki Ebihara, Department of Ophthalmology, Juntendo University School of Medicine, 2-1-1 Hongo, Bunkyo-ku, Tokyo 113-8421 Japan; ebihara@juntendo.ac.jp.

TABLE 1. Primary Antibodies

Antigen	Class	Dilution	Supplier
Anti-perlecan	Rabbit polyclonal	1/100	Seigaku, Tokyo Japan
Anti-Ki67	Rabbit polyclonal	1/200	Abcam, Cambridge UK
Anti-cytokeratin12	Goat polyclonal	1/200	Santa Cruz Biotech, Santa Cruz, CA
Anti-connexin43	Rabbit polyclonal	1/2000	Abcam
Anti-Notch1	Rabbit polyclonal	1/200	Abcam
Anti-Pax6	Mouse monoclonal	1/200	R&D Systems Minneapolis, MN

Hspg$^{+/Tg}$) were then created by mating the transgenic mice with heterozygous *Hspg2*$^{+/-}$ mice. The *Hspg2*$^{-/-}$-Tg mice exhibited normal cephalic development, and those mice were then maintained in a mixed genetic background of C57BL/6 and SVJ 129. In this study, we used 8- and 16-week-old *Hspg2*$^{-/-}$-Tg mice and *Hspg2*$^{+/+}$-Tg mice as well as wild-type (WT) mice, and the eyes of those mice were dissected and prepared for histologic or molecular analysis. All animal experiments in this study were performed in accordance with the guidelines set forth in the ARVO Statement for the Use of Animals in Ophthalmic and Vision Research.

Histologic Analysis

The excised mouse eyes were fixed in 20% formalin in phosphate-buffered saline (PBS) at 4°C overnight and then embedded in paraffin. Next, 3-μm-thick sections of the eyes were mounted on microslides (New Silane; Muto-Glass, Tokyo, Japan). Histologic examination was performed after Harris hematoxylin and eosin (H-E) staining. Histology of the corneas of the 8-week-old *Hspg2*$^{-/-}$-Tg and WT mice littermates was then compared by use of light microscopy (AX80; Olympus Corp., Tokyo, Japan).

Morphometric Measurements

For the morphometric measurements, corneal thicknesses were calculated in 8-week-old *Hspg2*$^{-/-}$-Tg and WT mice. Next, 3-μm-thick tissue sections of the cornea stained with H-E staining were viewed by light microscopy (40× magnification) with a computerized image analyzer (KS400; Carl Zeiss AG, Oberkochen, Germany), and measurements were made by use of a calibrated eyepiece graticule. Corneal thickness was measured in the central region of the serial sections of each eye. The mean thickness was then calculated by averaging those measurements. The epithelial, stromal, endothelial, and whole corneal thicknesses were then compared. The ratio of the epithelial cell layer thickness to the full corneal thickness was also calculated.

Examination by Transmission Electron Microscopy

For the transmission electron microscopy (TEM) examinations, the eyes of 8- and 16-week-old *Hspg2*$^{-/-}$-Tg and WT mice were dissected and fixed in cold 2.5% glutaraldehyde with PBS overnight at 4°C and then sectioned into small pieces. Those sections were then postfixed with 2% osmium tetroxide in the same buffer, dehydrated through a series of ethyl alcohol solutions, and embedded in Epon. All sections were examined by use of an electron microscope (H-7100; Hitachi, Tokyo, Japan) at an accelerating voltage of 75 kV.

Immunohistochemical Staining

Deparaffinized sections were washed in 100% ethanol and rehydrated with PBS. Antigen retrieval was performed by boiling the sections in 0.01 M citrate buffer (pH 6) for 10 minutes. Next, the slides were washed with PBS and blocked with 4% normal serum (species selected according to the secondary antibody) in PBS and 0.3% bovine serum albumin for 10 minutes at room temperature. The slides were incubated with primary antibody overnight at 4°C (Table 1), washed with PBS, incubated with the secondary antibodies, and counterstained with DAPI (H-1200; Vector Laboratories, Inc., Burlingame, CA). Ki67-positive cells were quantified by capturing the image of individual nuclei from *Hspg2*$^{-/-}$-Tg and WT sections processed in parallel and immunostained on the same slides. All sections were viewed with a fluorescence microscope (AxioVision 3.1; Carl Zeiss Meditec, Inc.) and confocal microscopy (TCS-SP5/TIRF; Leica Microsystems AG, Solms, Germany).

Assessment of Cell Death by TUNEL Assay

Deparaffinized sections were rehydrated through graded alcohols and then washed with PBS. The tissue sections were treated with proteinase K (80 μg/mL) for 20 minutes at room temperature. The slides were then washed twice with PBS. Next, the TUNEL assay (TUNEL in Situ Cell Death Detection Kit, fluorescein; Roche Diagnostics GmbH, Mannheim, Germany) was performed according to the manufacturer's instructions. Briefly, the sections were first counterstained with DAPI. The samples were then visualized by fluorescence microscopy, and images were obtained for quantitative analysis. TUNEL-positive cells were then quantified by capturing the image of individual nuclei from *Hspg2*$^{-/-}$-Tg and WT sections processed in parallel and immunostained on the same slides.

TABLE 2. Primers Used in RT-PCR

Gene	Primer	Primer Sequence
Ki67	Forward	5′-GCAGGAAGCAACAGATGAGAAGCC-3′
	Reverse	5′-GCTCAGGTGATACATGCCTCCTGC-3′
Active caspase3	Forward	5′-AGGTGGCAACGGAATTCGAGTC-3′
	Reverse	5′-ACACGGGATCTGTTTCTTTGCG-3′
Cytokeratin12	Forward	5′-TCTTCATGCTGGTGGTGTCCTTG-3′
	Reverse	5′-TCAAGAAACCAGGCCTCTGCATC-3′
Connexin43	Forward	5′-TCTTCATGCTGGTGGTGTCCTTG-3′
	Reverse	5′-CGATCCTTAACGCCCTTGAAGAAG-3′
Notch1	Forward	5′-GGAGGACCTCATCAACTCACATGC-3′
	Reverse	5′-CCGTTCTTCAGGAGCACAACAG-3′
Pax6	Forward	5′-AAGGATGTTGAACGGGCAGAC-3′
	Reverse	5′-TGTTGCTGGCAGCCATCTTG-3′
GAPDH	Forward	5′-AAGAGAGGCCCTATCCCAACTC-3′
	Reverse	5′-TTGTGGGTGCAGCGAACTTTATTG-3′

Analysis by Real-Time Polymerase Chain Reaction

Total RNA was isolated from the dissected corneas (NucleoSpin RNA II; Macherey-Nagel GmbH, KG, Duren, Germany) according to the manufacturer's instructions. cDNA was generated from 1.0 μg total RNA (ReverTra Ace-α; Toyobo Co., Ltd., Osaka, Japan). Real-time PCR was performed with SYBR green master mix (Fast SYBR Green Master Mix; Applied Biosystems, Inc. [ABI], Foster City, CA) on a commercial system (Prism 7500; ABI). In this study, we did not isolate the RNA from the epithelia but from the whole cornea. Therefore, the PCR analysis for the level of reduced expression of differentiation and developmental regulator molecules in *Hspg2*$^{-/-}$-Tg eyes may be semiquantitative, not absolutely quantitative. Primers sequences are listed in Table 2.

Results

Histologic Analysis of the *Hspg2*$^{-/-}$-Tg Eyes

The eyes of 8-week-old *Hspg2*$^{-/-}$-Tg mice that were approximately the same body weight and length as WT mice exhibited microphthalmos and a small palpebral fissure (Fig. 1A). Under light microscopy at low magnification, the *Hspg2*$^{-/-}$-Tg eyes stained with H-E staining also exhibited microphthalmos (Figs. 1B, 1C). Under high magnification, the *Hspg2*$^{-/-}$-Tg eyes showed a thinner corneal epithelium compared with that of the WT eyes (Figs. 1D, 1E). The localization of perlecan was examined by immunostaining with specific antibody for their core protein. Eight-week-old WT and *Hspg2*$^{-/-}$-Tg mice were stained with anti-perlecan antibody (Alexa488, green), and the corneal nuclei were stained with DAPI (blue). Perlecan was strongly expressed in the corneal epithelial BM of the WT mice (Fig. 1F). However, the expression of perlecan was not recognized in the corneal epithelium of the *Hspg2*$^{-/-}$-Tg mice (Fig. 1G).

Analysis by TEM

TEM was performed to further examine the corneal morphology in the *Hspg2*$^{-/-}$-Tg and WT mice. The corneal epithelia from WT mice and *Hspg2*$^{-/-}$-Tg, 8 weeks (Figs. 2A, 2B) and 16 weeks (Figs. 2C, 2D) of age, were analyzed by TEM. At 8 and 16 weeks of age, the *Hspg2*$^{-/-}$-Tg mice showed thinner corneal epithelia compared with the WT mice. Eight-week-old WT mice showed 9 to 10 corneal epithelial layers (Fig. 2A). In contrast, the 8-week-old *Hspg2*$^{-/-}$-Tg mice showed thinner undifferentiated wing cell layers compared with the WT mice (Fig. 2B). Corneal wing-cell layers of the 16-week-old *Hspg2*$^{-/-}$-Tg mice were thinner and undifferentiated compared with those of the WT mice. As the ages of the mice progressed, the *Hspg2*$^{-/-}$-Tg mice showed a thinner corneal epithelium compared with that of the WT mice (Fig. 2A-D). Under high magnification, no significant difference was observed between the *Hspg 2*$^{-/-}$ Tg mice and WT mice in regard to the structure of superficial cells (Figs. 2E, 2F), basal cells (Figs. 2G, 2H), and epithelial BM (Figs. 2I, 2J).

In the corneal stromal layer, the keratocytes were localized between stromal lamellae, with no significant difference found between the 8-week-old *Hspg2*$^{-/-}$-Tg and WT mice (Figs. 3A, 3B). Under high magnification, cross-sections of the collagen fibers from the *Hspg2*$^{-/-}$-Tg and WT mice demonstrated parallel bundles of a regular diameter (Figs. 3C, 3D). Under low magnification, no significant difference was observed between the *Hspg2*$^{-/-}$-Tg and WT mice as to the thickness of the endothelial layers (Figs. 3E, 3F). Under high magnification, Descemet's membrane was found to be composed of electron-dense material in both the *Hspg2*$^{-/-}$-Tg and WT mice (Figs. 3G, 3H). The corneal endothelium was found to have some

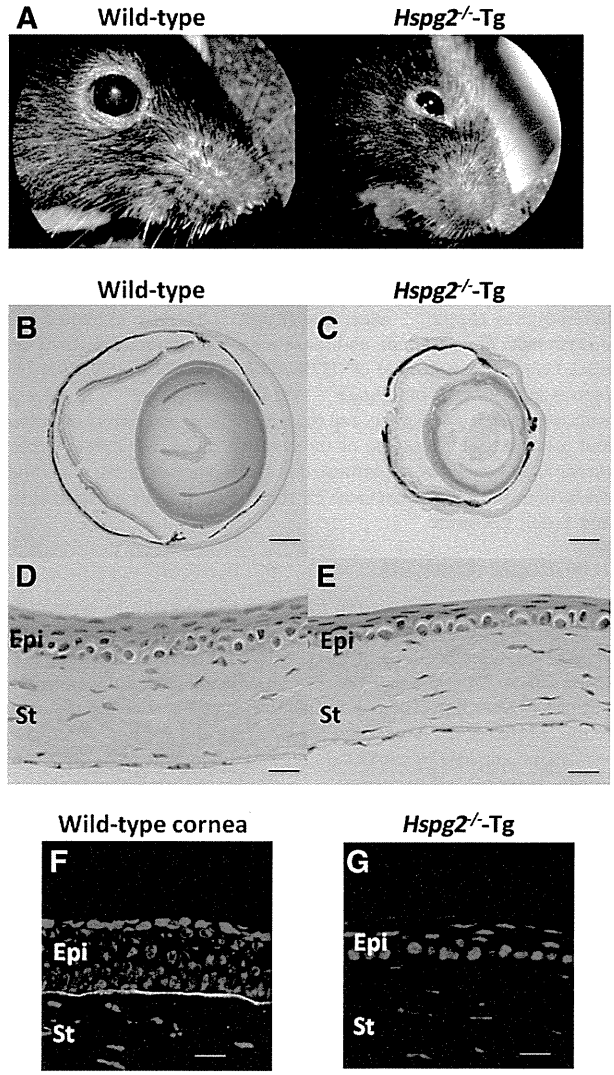

Figure 1. Histologic analysis. Representative macroscopic images of the eye in situ (**A**). H-E-stained sections (**B–E**) show the histologic features of whole eyes visualized by light microscopy at low (**B**, **C**) and high (**D**, **E**) magnifications. The 8-week-old *Hspg2*$^{-/-}$-Tg mice had microphthalmos, whereas the WT mice did not (**A–C**). The corneal epithelium of the 8-week-old *Hspg2*$^{-/-}$-Tg mice thinner than that of the WT mice (**D**, **E**). Immunohistochemical staining of perlecan in the corneas of the WT and the *Hspg2*$^{-/-}$-Tg mice (**F**, **G**). Perlecan (Alexa 488, *green*) was strongly expressed in the corneal epithelial basement membrane of the WT mice (**F**). However, the expression of perlecan was not recognized in the corneal epithelium of the *Hspg2*$^{-/-}$-Tg mice (**G**). Epi, epithelium; St, stroma. Scale bars: (**B**, **C**) 600 μm; (**D**, **E**) 40 μm; (**F**, **G**) 30 μm.

desmosomes and gap junctions, with no significant difference found between the *Hspg2*$^{-/-}$-Tg and WT mice (Figs. 3I, J).

Corneal Thickness Morphometry

The thickness of the corneal epithelium was examined in the 8-week-old mice, as that is the age at which the development of the corneal epithelium is complete. Histologic examination of those mice revealed that the corneal epithelial thickness was markedly thinned in the *Hspg2*$^{-/-}$-Tg mice. The corneal thickness of the central region was then calculated (Fig. 4A). The thickness of the central whole corneal cell layers was found to

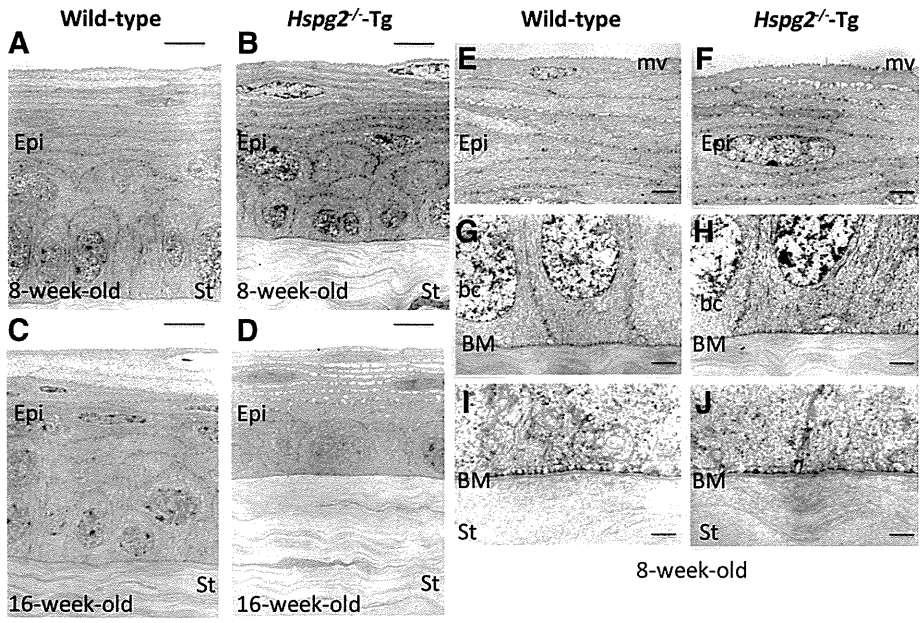

FIGURE 2. TEM of the corneal epithelium. TEM images show ultrastructural features of corneal epithelium from WT (**A**, **C**, **E**, **G**, **I**) and *Hspg2*$^{-/-}$-Tg (**B**, **D**, **F**, **H**, **J**) mice. Corneal epithelia of the 8- and 16-week-old *Hspg2*$^{-/-}$-Tg mice (**B**, **D**) were thinner and had thinner wing cell layers compared with those of the WT mice (**A**, **C**). As the ages of the mice progressed, the corneal epithelium of the 16-week-old *Hspg2*$^{-/-}$-Tg mice became thinner and the wing cell layer was undifferentiated compared with that of the WT mice (**D**). Under high magnification, no significant difference was observed between the *Hspg2*$^{-/-}$-Tg mice and WT mice in regard to the structure of the superficial cells (**E**, **F**), basal cells (**G**, **H**), and epithelial basement membrane (**I**, **J**). Epi, epithelium; St, stroma; mv, microvilli; bc, basal cell, BM, corneal basement membrane. Scale bar: (**A–D**) 5 μm; (**E-H**) 2 μm; (**I**, **J**) 0.5 μm.

be 25.6% thinner in the *Hspg2*$^{-/-}$-Tg mice (on average, 85.12 μm thick compared with 114.53 μm in the WT mice; $n = 6$; $P = 0.0411$). The thickness of the central epithelial cell layers was found to be 45.5% thinner in the *Hspg2*$^{-/-}$-Tg mice (on average, 18.51 μm thick compared with 33.94 μm in the WT mice; $n = 6$; $P = 0.0022$). The average thicknesses of the central corneal stromal layers and endothelial layers were not significantly different between the *Hspg2*$^{-/-}$-Tg and WT mice. Because of the microphthalmos of the eyes of the *Hspg2*$^{-/-}$-Tg mice, we calculated the comparison of the ratio of the epithelial cell layer thickness to the full central corneal thickness in the central region (Fig. 4B). The ratio of the central epithelial cell layer thickness to the central whole corneal thickness was found to be significant lower in the *Hspg2*$^{-/-}$-Tg mice, 22.6% compared with 29.4% in the WT mice ($n = 6$, $P = 0.0043$). These findings suggest that the corneal epithelial cell layer in the *Hspg2*$^{-/-}$-Tg mouse is thinner regardless of the microphthalmos.

Proliferation and Cell Death in *Hspg2*$^{-/-}$-Tg Corneal Epithelium

We posited that the findings of thinner corneal epithelium in the 8-week-old *Hspg2*$^{-/-}$-Tg mice could be the result of a decrease in cell proliferation or an increase in cell death. To discern between these two possibilities, immunostaining was performed to investigate the number of Ki67-positive (Figs. 5A1, A2) and TUNEL-positive (Figs. 5D1, 5D2) cells. The Ki67 antigen was designated as a marker for cell proliferation, and the number of Ki67-positive cells was scored across the entire section of the corneal epithelium. The average ratio of Ki67-positive cells to basal cells was 12% per section in the *Hspg2*$^{-/-}$-Tg epithelium, compared with 21% in the WT epithelium ($n = 6$; $P = 0.0087$; Fig. 5B). Real-time PCR for Ki67 showed a 67% decrease in RNA levels in the *Hspg2*$^{-/-}$-Tg epithelium ($n = 5$; $P = 0.0159$; Fig. 5C).

TUNEL assay assessment of cell death revealed a very small number of TUNEL-positive cells (<0.3%) per corneal section in

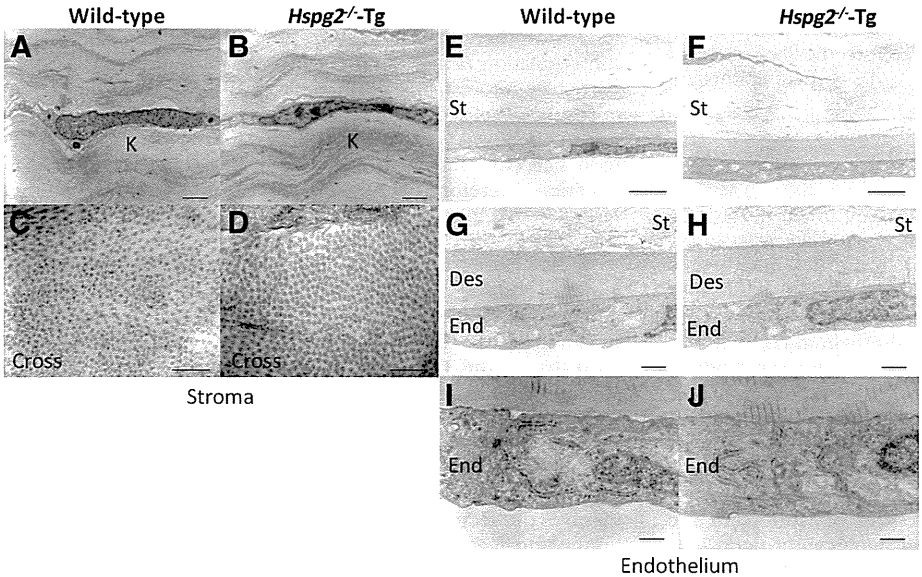

FIGURE 3. Electron microscopy of corneal stroma and endothelium. Keratocytes (**A**, **B**). Collagen fibers cut in cross-section (**C**, **D**). Stroma and corneal endothelium observed under low magnification (**E**, **F**). Descemet's membrane observed under high magnification (**G**, **H**). Corneal endothelium observed under high magnification (**I**, **J**). No significant differences were found between the 8-week-old *Hspg2*$^{-/-}$-Tg mice and WT mice in regard to the construction of the stroma and endothelium. K, keratocytes; St, stroma; Des, Descemet's membrane; End, endothelium. Scale bar: (**A**, **B**) 2 μm; (**C**, **D**, **I**, **J**) 0.5 μm; (**E**, **F**) 5 μm; (**G**, **H**) 1 μm.

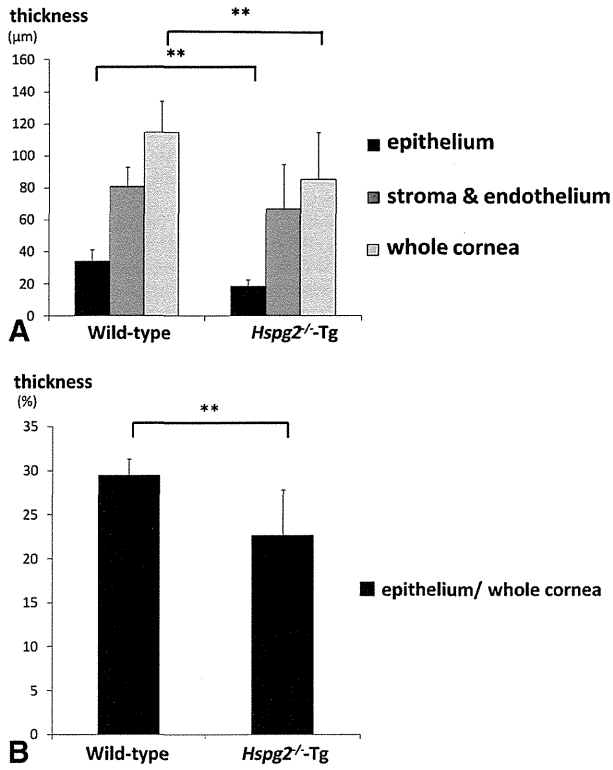

FIGURE 4. Morphometry of corneal thickness. Comparison of central corneal thickness. (**A**) The central corneal epithelial cell layer of the 8-week-old *Hspg2*$^{-/-}$-Tg mice was significantly thinner than that of the 8-week-old WT mice (n = 6; P = 0.0022). The full central corneal thickness was significantly thinner in the 8-week-old *Hspg2*$^{-/-}$-Tg mice compared with that in the 8-week-old WT mice (n = 6; P = 0.0411). Comparison of the ratio of the epithelial cell layer thickness to the full corneal thickness measured at the central cornea (**B**). The ratio of epithelial cell layer thickness to full corneal thickness was significantly lower in the *Hspg2*$^{-/-}$-Tg mice than in the WT mice (n = 6; P = 0.0043; Mann-Whitney U test: $^{*}P < 0.05$, $^{**}P < 0.01$, $^{***}P < 0.0001$).

both the *Hspg2*$^{-/-}$-Tg and WT epithelium (Fig. 5E), and there was no increase in RNA levels of active caspase3 of the apoptosis marker in both *Hspg2*$^{-/-}$-Tg and WT corneal epithelium (Fig. 5F), thus indicating that the loss of perlecan did not lead to a significant change in the rate of apoptosis. Therefore, the likely cause of the thinning of the 8-week-old *Hspg2*$^{-/-}$-Tg corneal epithelium was determined to be reduced cell proliferation.

Effect of Perlecan Deficiency on the Expression of Markers of Corneal Epithelial Differentiation

The expression of cytokeratin12 (K12), a corneal differentiation marker, in the 8-week-old *Hspg2*$^{-/-}$-Tg mice was significantly decreased compared with that in the WT mice examined by immunohistochemistry (Figs. 6A1, A2). Real-time PCR for K12 in the *Hspg2*$^{-/-}$-Tg epithelium showed a 54% decrease in RNA levels compared with the WT epithelium (n = 5; P = 0.4698; Fig. 6E). Connexin43 (Cx43), a gap junction protein, was found to be present in the corneal basal cell layers in the WT epithelium, but was absent in the *Hspg2*$^{-/-}$-Tg epithelium by immunohistochemistry (Figs. 6B1, 6B2). Real-time PCR for Cx43 in the *Hspg2*$^{-/-}$-Tg epithelium showed a 41% decrease in RNA levels compared with that in the WT epithelium (n = 5; P = 0.4698; Fig. 6E). The expression of Notch1 in the *Hspg2*$^{-/-}$-Tg corneal epithelium was significantly decreased compared with that of the WT epithelium by immunohistochemistry (Figs. 6C1, 6C2). Real-time PCR showed that the *Hspg2*$^{-/-}$-Tg mutation caused a significantly decrease in Notch1 RNA levels in the corneal epithelium, compared with that in the WT mice (n = 5; P = 0.0159; Fig. 6E). The expression of Pax6, a developmental regulator marker, was shown by immunohistochemistry to be significantly decreased in the corneal epithelium in the *Hspg2*$^{-/-}$-Tg mice compared with that of the WT mice (Figs. 6D1, 6D2). Real-time PCR for Pax6 in the *Hspg2*$^{-/-}$-Tg epithelium showed a significant decrease in RNA levels compared with that in the WT epithelium (n = 5; P = 0.0159; Fig. 6E).

DISCUSSION

In this study, perlecan was identified in corneal epithelial BM and the epithelium was shown to be thin and poorly differentiated in perlecan-deficient mice (*Hspg2*$^{-/-}$-Tg) and accompanied by the downregulation of Ki67, K12, Cx43, Notch1, and Pax6. However, the gross morphology of the corneal epithelium was not retarded in the *Hspg2*$^{-/-}$-Tg mice, suggesting that perlecan is not critically necessary in this process. Therefore, perlecan may be essential for the structure but not the development of corneal epithelium. In normal corneal epithelium, epithelial cells in the last phase of their differentiation undergo apoptosis as they reach the superficial cell layer. Since the cell death rate of the corneal epithelial cells in the *Hspg2*$^{-/-}$-Tg mice was similar to that in WT mice, the failure of those cells to form multilayered corneal epithelium must be due to the apparent decrease in the proliferation and differentiation rates in corneal epithelial cells. In this present study, we revealed that the expression of Ki67, K12, Cx43, Notch 1, and Pax6, which are markers of cell proliferation and differentiation, was reduced in the *Hspg2*$^{-/-}$-Tg mice, compared with that of the WT mice. Therefore, our findings revealed that perlecan in the BM of corneal epithelium may be critical for normal epithelial formation and terminal differentiation.

It has been reported that K12 is essential for the differentiation and maintenance of corneal epithelium integrity.,[18,19] Targeted deletion of K12 in a mouse model showed fewer cellular layers in the corneal epithelium and corneal fragility.[19] The findings of this study showed that downregulation of the expression of K12 at protein and RNA levels may be one of the causes of aberrant differentiation in the *Hspg2*$^{-/-}$-Tg corneal epithelium. From another aspect, it has been reported that the gap junction marker Cx43 mediates the intercellular diffusion ions and other small molecules,[20-22] thereby contributing to the regulation of tissue differentiation and homeostasis.[23] Of particular interest, the expression of Cx43 was noted in the corneal epithelial basal cells in the WT corneal epithelium, but not in the *Hspg2*$^{-/-}$-Tg epithelium, thus suggesting that the basal cell environment is impaired by gap junction functional decline. Therefore, the downregulation of Cx43 in the *Hspg2*$^{-/-}$-Tg mice most likely impairs the differentiation and structure of the corneal epithelium.

It has been reported that the Notch signaling pathway, another corneal homeostasis marker, limits cell proliferation and promotes differentiation.[24-27] In this study, the expression of Notch1 was decreased in the *Hspg2*$^{-/-}$-Tg mice, compared with that in the WT mice. Recently, Vauclair et al.[27] demonstrated that Notch1-deficient corneal cells lose their ability to heal and repair wounded corneal epithelium. The findings of that study showed that instead of generating new corneal epithelium after injury, those cells repair the wound by forming a hyperproliferative epidermislike epithelium. This process involves the secretion of FGF-2 through Notch1 signaling in the epithelium.[27] It is well known that FGF-2 is a growth factor of corneal epithelial cells.[28,29] Loss of Notch 1 in the corneal

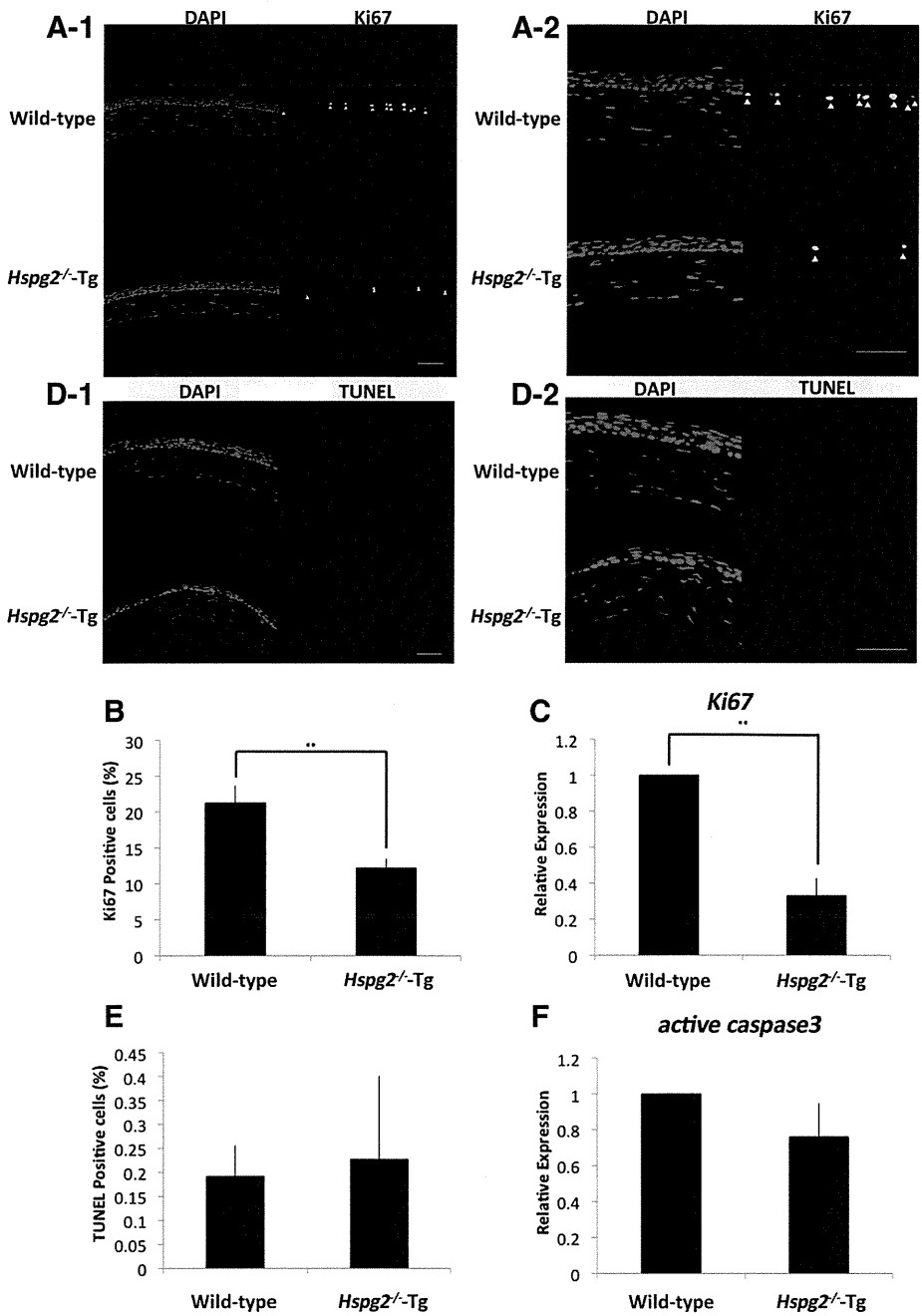

FIGURE 5. Proliferation and cell death in the *Hspg2*$^{-/-}$-Tg corneal epithelium. Immunohistochemistry showed a decreased number of cells containing Ki67 (Alexa488, *green*, *white arrow*) in the 8-week-old *Hspg2*$^{-/-}$-Tg versus WT corneal epithelium (DAPI, *blue*; **A1**, **A2**). The percentage of Ki67-positive cells in the corneal epithelium showed a 9.0% decrease in the *Hspg2*$^{-/-}$-Tg mice (±SEM, $n = 6$, $P = 0.0087$; **B**). Quantification of RNA levels for Ki67 in the corneal epithelium (±SEM; $n = 5$; $P = 0.0159$; **C**). In the superficial corneal cells, there was almost no TUNEL-positive staining (**D1**, **D2**). The percentage of TUNEL-positive cells in the corneal epithelium (±SEM, $n = 6$; **E**). Quantification of RNA levels for active caspase3 in the corneal epithelium (±SEM; $n = 5$; **F**; Mann-Whitney U test: $^{*}P < 0.05$, $^{**}P < 0.01$, $^{***}P < 0.0001$). Scale bar: 50 μm. Low magnification: **A1**, **D1**; high magnification: **A2**, **D2**.

epithelium resulted first in upregulation of FGF-2 by the corneal epithelium, suggesting that Notch1 signaling repressed its expression.[27] Despite the decreased expression of Notch1, a hyperproliferative change of corneal epithelium was not observed in the *Hspg2*$^{-/-}$-Tg mice. Since FGF-2 is a ligand of perlecan, there may be a possibility that a high dose of FGF-2 could not be maintained in the BM of the corneal epithelium of *Hspg2*$^{-/-}$-Tg mice.[30–35] Reportedly, FGF-7 is also a ligand of perlecan.[1] In a recent study, Lovicu et al.[36] showed hyperproliferation of embryonic corneal epithelial cells in transgenic mice engineered to overexpress human FGF-7 in the eye. Chikama et al.[37] analyzed the effects of excess FGF-7 on both the proliferation and differentiation of corneal epithelium in an FGF-7 transgenic mouse model in which cornea-specific FGF-7 was overexpressed. In that study, the mice exhibited epithelial hyperplasia, accompanied by the downregulation of K12. According to these results, the mechanism of the poor differentiation of the epithelium in *Hspg2*$^{-/-}$-Tg mice is due to the lack of the FGF-2 or FGF-7 that links to perlecan in the BM. Therefore, the strong correlation between the presence of perlecan in the BM and the formation of normal corneal epithelium suggests that perlecan functions as a reservoir for soluble factors involved in the proliferation and differentiation of corneal epithelial cells.

It should be noted that the *Hspg2*$^{-/-}$-Tg mice had microphthalmos. This condition has been reported in Pax6-deficient mice.[38–41] These reports suggest that Pax6 is a key developmental regulator and that it is generally essential for morphogenesis in the eye. Pax6 has autonomous roles in all eye tissues, where it is expressed at several developmental stages. Re-

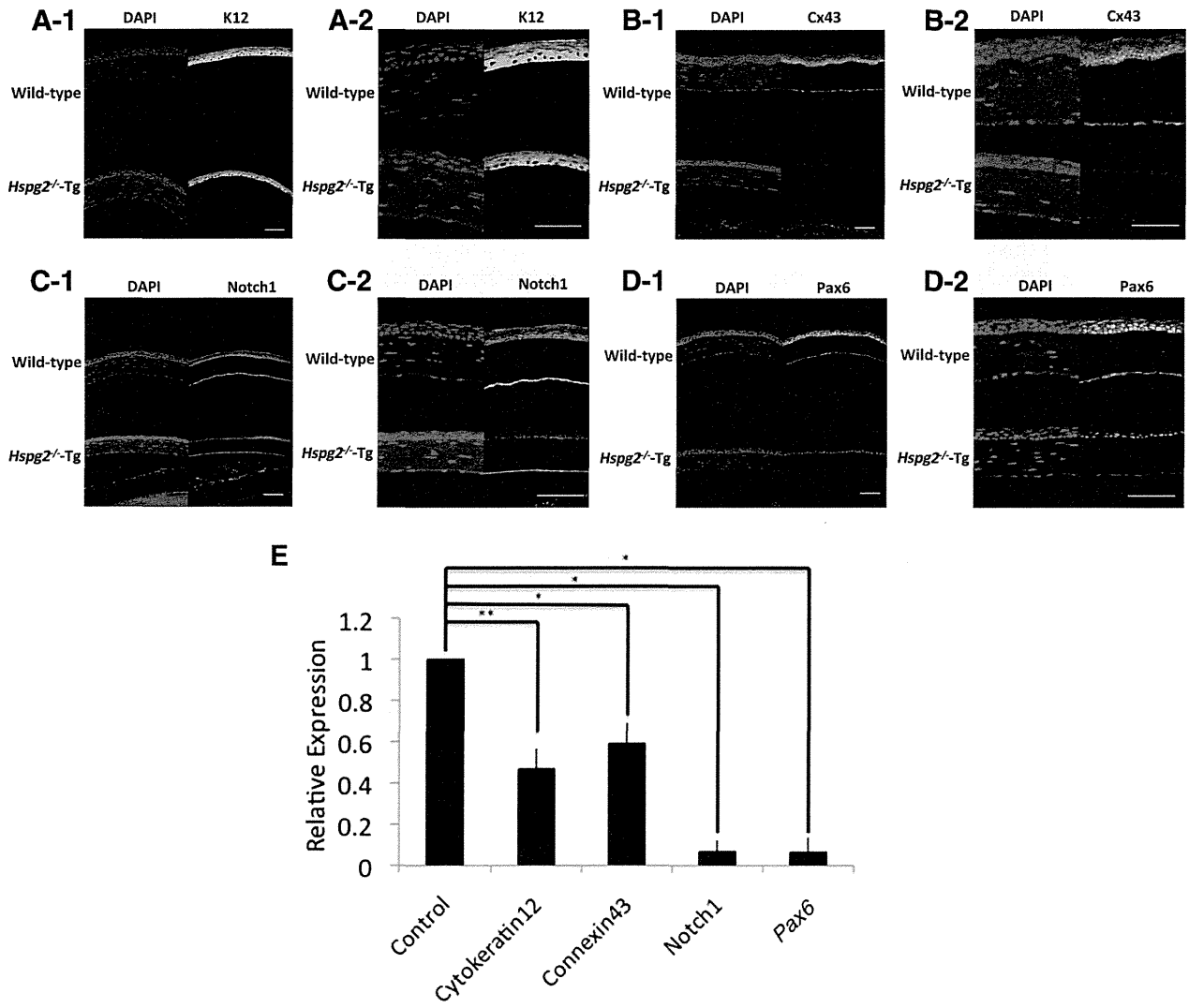

FIGURE 6. Expression of differentiation and developmental regulator markers in the 8-week-old *Hspg2*$^{-/-}$-Tg corneal epithelium demonstrated that the expression of cytokeratin12 (K12) in the *Hspg2*$^{-/-}$-Tg epithelium was significantly decreased compared with that in the WT epithelium (**A1**, **A2**). *Hspg2*$^{-/-}$-Tg corneal epithelium showed no expression of Connexin43 (Cx43; **B1**, **B2**). The expression of Notch1 in *Hspg2*$^{-/-}$-Tg corneal epithelium was significantly decreased compared with that in the WT epithelium (**C1**, **C2**). *Hspg2*$^{-/-}$-Tg corneal epithelium showed decreased Pax6 expression compared with that in the WT epithelium (**D1**, **D2**). Quantification of RNA levels for differentiation and developmental regulator markers in corneal epithelium (±SEM, $n = 5$; **E**; Mann-Whitney U test: $^{*}P < 0.05$, $^{**}P < 0.01$, $^{***}P < 0.0001$). Scale bar: 50 μm. Low magnification: **A1**, **B1**, **C1**, **D1**; high magnification: **A2**, **B2**, **C2**, **D2**.

cently, a report by Garcia-Villegas et al.[42] revealed that Pax6 is the earlier differentiation marker expressed by corneal epithelial cells and that it is the main driver of the differentiation of corneal epithelial cells, as the expression of Pax6 promotes the differentiation of corneal epithelial cells. On the other hand, transgenic mice overexpressing Pax6 in the corneal epithelium also showed abnormal epithelial cell morphology. These results indicate that a correct Pax6 dosage for the normal development of corneal epithelium may be important. In this present study, we demonstrated that the corneal epithelium of *Hspg2*$^{-/-}$-Tg mice was thinner and not well differentiated and that the phenotypes became more severe with age. The corneal epithelial phenotype was similar to that of Pax6-deficient mice. Thus, the downregulation of Pax6 in the corneal epithelium of *Hspg2*$^{-/-}$-Tg mice is likely to be a factor in the observed microphthalmos and thinner epithelium. We theorize that the downregulation of K12, Cx43, Notch1, and Pax6 probably occurs to prevent the proliferation and the differentiation from basal cells to wing cells, thus making the corneal epithelium of *Hspg2*$^{-/-}$-Tg mice thinner than that of WT mice with downregulation of the expression of Ki67.

In summary, by using perlecan-deficient mice (*Hspg2*$^{-/-}$-Tg) we demonstrated for the first time that perlecan is essential for the structure of corneal epithelium, as it controls the expression of markers for the proliferation or differentiation of corneal epithelial cells. Our findings revealed that perlecan in the BM of corneal epithelium were critical for normal epithelial structure and terminal differentiation.

Acknowledgments

The authors thank Glenn Longenecker and Ashok B. Kulkarni for help in creating the mutant mice, Yoshihiko Yamada for critical reading of the manuscript, and Saori Ito for secretarial assistance.

References

1. Knox SM, Whitelock JM. Perlecan: how does one molecule do so many things? *Cell Mol Life Sci.* 2006;63:2435-2445.
2. Murdoch AD, Dodge GR, Cohen I, Tuan RS, Iozzo RV. Primary structure of the human heparin sulfate proteoglycan from basement membrane (HSPG2/perlecan): a chimeric molecule with multiple domains homologous to the low density lipoprotein receptor, laminin, neural cell adhesion molecules, and epidermal growth factor. *J Biol Chem.* 1992;267:8544-8557.
3. Noonan DM, Fulle A, Valente P, et al. The complete sequence of perlecan, a basement membrane heparan sulfate proteoglycan, reveals extensive similarity with laminin A chain, low density lipoprotein-receptor, and the neural cell adhesion molecule. *J Biol Chem.* 1991;26:22939-22947.
4. Hassell JR, Robey PG, Barrach HJ, et al. Isolation of a heparan sulfate-containing proteoglycan from basement membrane. *Proc Natl Acad Sci USA.* 1980;77:4494-4498.
5. Iozzo RV. Perlecan: a gem of a proteoglycan. *Matrix Biol.* 1994; 14:203-208.
6. Iozzo RV. Basement membrane proteoglycans: from cellar to ceiling. *Nat Rev Mol Cell Biol.* 2005;6:646-656.
7. Whitelock JM, Iozzo RV. Heparan sulfate: a complex polymer charged with biological activity. *Chem Rev.* 2005;105:2745-2764.
8. Handler M, Yurchenco PD, Iozzo RV. Developmental expression of perlecan during murine embryogenesis. *Dev Dyn.* 1997;210:130-145.
9. Knox S, Melrose J, Whitelock J. Electrophoretic, biosensor, and bioactivity analyses of perlecans of different cellular origins. *Proteomics.* 2001;1:1534-1541.
10. Jiang X, Couchman JR. Perlecan and tumor angiogenesis. *J Histochem Cytochem.* 2003;51:1393-1410.
11. Zhou Z, Wang J, Cao R, et al. Impaired angiogenesis, delayed wound healing and retarded tumor growth in perlecan heparan sulfate-deficient mice. *Cancer Res.* 2004;64:4699-4702.
12. Arikawa-Hirasawa E, Watanabe H, Takami H, Hassell JR, Yamada Y. Perlecan is essential for cartilage and cephalic development. *Nat Genet.* 1999;23:354-358.
13. Xu Z, Ichikawa N, Kosaki K, et al. Perlecan deficiency causes muscle hypertrophy, a decrease in myostatin expression, and changes in muscle fiber composition. *Matrix Biol.* 2010;29:461-470.
14. Rossi M, Morita H, Sormunen R, et al. Heparan sulfate chains of perlecan are indispensable in the lens capsule but not in the kidney. *EMBO J.* 2003;22:236-245.
15. Sher I, Zisman-Rozen S, Eliahu L, et al. Targeting perlecan in human keratinocytes reveals novel roles for perlecan in epidermal formation. *J Biol Chem.* 2006;281:5178-5187.
16. Kabosova A, Azar DT, Bannikov GA, et al. Compositional differences between infant and adult human corneal basement membranes. *Invest Ophthalmol Vis Sci.* 2007;48:4989-4999.
17. Costell M, Gustafsson E, Aszódi A, et al. Perlecan maintains the integrity of cartilage and some basement membranes. *J Cell Biol.* 1999;147:1109-1122.
18. Chaloin-Dufau C, Sun TT, Dhouailly D. Appearance of the keratin pair K3/K12 during embryonic and adult corneal epithelial differentiation in the chick and in the rabbit. *Cell Differ Dev.* 1990;32: 97-108.
19. Kao WW, Liu CY, Converse RL, et al. Keratin 12-deficient mice have fragile corneal epithelia. *Invest Ophthalmol Vis Sci.* 1996;37: 2572-2584.
20. Kimura K, Teranishi S, Nishida T. Establishment of human corneal epithelial cells stably expressing human connexin43. *Exp Eye Res.* 2010;90:4-9.
21. Ko JA, Yanai R, Morishige N, Takezawa T, Nishida T. Upregulation of connexin43 expression in corneal fibroblasts by corneal epithelial cells. *Invest Ophthalmol Vis Sci.* 2009;50:2054-2060.
22. Yang HS, Lu XH, Chen DY, et al. Upregulated expression of connexin43 in spinal ligament fibroblasts derived from patients presenting ossification of the posterior longitudinal ligament. *Spine* (Phila Pa 1976). 2011;36:2267-74.
23. Kumar NM, Gilula NB. The gap junction communication channel. *Cell.* 1996;84:381-388.
24. Ma A, Boulton M, Zhao B, Connon C, Cai J, Albon J. A role for notch signaling in human corneal epithelial cell differentiation and proliferation. *Invest Ophthalmol Vis Sci.* 2007;48:3576-3585.
25. Djalilian AR, Namavari A, Ito A, et al. Down-regulation of Notch signaling during corneal epithelial proliferation. *Mol Vis.* 2008;14: 1041-1049.
26. Thomas PB, Liu YH, Zhuang FF, et al. Identification of Notch-1 expression in the limbal basal epithelium. *Mol Vis.* 2007;13:337-344.
27. Vauclair S, Majo F, Durham AD, et al. Corneal epithelial cell fate is maintained during repair by Notch1 signaling via the regulation of vitamin A metabolism. *Dev Cell.* 2007;13:242-253.
28. Hu C, Ding Y, Chen J, et al. Basic fibroblast growth factor stimulates epithelial cell growth and epithelial wound healing in canine corneas. *Vet Ophthalmol.* 2009;12:170-175.
29. Wang X, Zhou X, Ma J, et al. Effects of keratinocyte growth factor-2 on corneal epithelial wound healing in a rabbit model of carbon dioxide laser injury. *Biol Pharm Bull.* 2010;33:971-976.
30. Friesel RE, Maciag T. Molecular mechanisms of angiogenesis: fibroblast growth factor signal transduction. *FASEB J.* 1995;9:919-925.
31. Takehara K. Growth regulation of skin fibroblasts. *J Dermatol Sci.* 2000;24(suppl 1):S70-S77.
32. Aviezer D, Hecht D, Safran M, et al. Perlecan, basal lamina proteoglycan, promotes basic fibroblast growth factor-receptor binding, mitogenesis, and angiogenesis. *Cell.* 1994;79:1005-1013.
33. Knox S, Merry C, Stringer S, Melrose J, Whitelock J. Not all perlecans are created equal: interactions with fibroblast growth factor (FGF) 2 and FGF receptors. *J Biol Chem.* 2002;277:14657-14665.
34. Whitelock JM, Murdoch AD, Iozzo RV, Underwood PA. The degradation of human endothelial cell-derived perlecan and release of bound basic fibroblast growth factor by stromelysin, collagenase, plasmin, and heparanases. *J Biol Chem.* 1996;271:10079-10086.
35. Whitelock JM, Graham LD, Melrose J, et al. Human perlecan immunopurified from different endothelial cell sources has different adhesive properties for vascular cells. *Matrix Biol.* 1999;18: 163-178.
36. Lovicu FJ, Kao WW, Overbeek PA. Ectopic gland induction by lens-specific expression of keratinocyte growth factor (FGF-7) in transgenic mice. *Mech Dev.* 1999;88:43-53.
37. Chikama T, Liu CY, Meij JT, et al. Excess FGF-7 in corneal epithelium causes corneal intraepithelial neoplasia in young mice and epithelium hyperplasia in adult mice. *Am J Pathol.* 2008;172:638-649.
38. Chanas SA, Collinson JM, Ramaesh T, et al. Effects of elevated Pax6 expression and genetic background on mouse eye development. *Invest Ophthalmol Vis Sci.* 2009;50:4045-4059.
39. Favor J, Bradley A, Conte N, et al. Analysis of Pax6 contiguous gene deletions in the mouse, Mus musculus, identifies regions distinct from Pax6 responsible for extreme small-eye and belly-spotting phenotypes. *Genetics.* 2009;182:1077-1088.
40. Shaham O, Smith AN, Robinson ML, et al. Pax6 is essential for lens fiber cell differentiation. *Development.* 2009;136:2567-2578.
41. Wolf LV, Yang Y, Wang J, et al. Identification of pax6-dependent gene regulatory networks in the mouse lens. *PLoS One.* 2009;4: e4159.
42. García-Villegas R, Escamilla J, Sánchez-Guzmán E, et al. Pax-6 is expressed early in the differentiation of a corneal epithelial model system. *J Cell Physiol.* 2009;220:348-356.

ARTICLE IN PRESS
JNS-12138; No of Pages 5
Journal of the Neurological Sciences xxx (2012) xxx–xxx
Contents lists available at SciVerse ScienceDirect
Journal of the Neurological Sciences
journal homepage: www.elsevier.com/locate/jns

A novel mutation in SCN4A causes severe myotonia and school-age-onset paralytic episodes

Harumi Yoshinaga [a,*], Shunichi Sakoda [b], Jean-Marc Good [c], Masanori P. Takahashi [c], Tomoya Kubota [c], Eri Arikawa-Hirasawa [d], Tomohiko Nakata [e], Kinji Ohno [e], Tetsuro Kitamura [f], Katsuhiro Kobayashi [a], Yoko Ohtsuka [a]

[a] Department of Child Neurology, Okayama University Graduate School of Medicine, Dentistry, and Pharmaceutical Sciences, Okayama, Japan
[b] Department of Neurology, Kagoshima University Graduate School of Medical and Dental Sciences, Medical School, Kagoshima, Japan
[c] Department of Neurology, Osaka University Graduate School of Medicine, Osaka, Japan
[d] Department of Neurology, Juntendo University School of Medicine, Tokyo, Japan
[e] Division of Neurogenetics, Center for Neurological Diseases and Cancer, Nagoya University Graduate School of Medicine, Aichi, Japan
[f] Department of Pediatrics, Nipponkokan Fukuyama Hospital, Hiroshima, Japan

ARTICLE INFO

Article history:
Received 27 June 2011
Received in revised form 30 November 2011
Accepted 22 December 2011
Available online xxxx

Keywords:
Channelopathy
Na channel
Skeletal muscle
Activation
Slow inactivation
Schwarz–Jampel syndrome
SCN4A

ABSTRACT

Mutations in the pore-forming subunit of the skeletal muscle sodium channel (*SCN4A*) are responsible for hyperkalemic periodic paralysis, paramyotonia congenita and sodium channel myotonia. These disorders are classified based on their cardinal symptoms, myotonia and/or paralysis. We report the case of a Japanese boy with a novel mutation of *SCN4A*, p.I693L, who exhibited severe episodic myotonia from infancy and later onset mild paralytic attack. He started to have apneic episodes with generalized hypertonia at age of 11 months, then developed severe episodic myotonia since 2 years of age. He presented characteristic generalized features which resembled Schwarz–Jampel syndrome. After 7 years old, paralytic episodes occurred several times a year. The compound muscle action potential did not change during short and long exercise tests. Functional analysis of the mutant channel expressed in cultured cell revealed enhancement of the activation and disruption of the slow inactivation, which were consistent with myotonia and paralytic attack. The severe clinical features in his infancy may correspond to myotonia permanence, however, he subsequently experienced paralytic attacks. This case provides an example of the complexity and overlap of the clinical features of sodium channel myotonic disorders.

1. Introduction

To date, over 40 different mutations causing Na channelopathies of the skeletal muscle have been reported in *SCN4A* gene, which encodes for the pore-forming alpha-subunit of skeletal muscle sodium channel [1,2]. The Na channelopathies of the skeletal muscle are clinically classified into hyperkalemic periodic paralysis, paramyotonia congenita, or sodium channel myotonia on the basis of their clinical phenotype. However, phenotypic variability and marked overlap in symptoms have been reported [3–6]. The cases with severe phenotype in the neonatal period highlight the high clinical variability of sodium channelopathies [7,8]. The electrophysiological studies using heterologously expressed channels have shown that the missense mutations produces a gain-of-function defect of the fast gating such as disrupted fast inactivation and enhanced activation, which should result in increased excitability of the muscle membrane. It has been revealed that not only the defect of fast gating but also that of slow inactivation predisposes to paralytic attack, one of the clinical features of Na channelopathies [9,10].

In this report, we present a Japanese boy with skeletal dysplasia who exhibited very severe myotonia in infancy and mild paralytic attack after seven years of age. We identified a novel mutation in the intracellular loop linking segments 4–5 of domain II in *SCN4* and found that the heterologously expressed mutant channel showed enhancement of the activation and disruption of the slow inactivation.

2. Case report

2.1. Clinical features

The patient was delivered naturally and without complications. There is no family history of neuromuscular disease. Seven days after birth, he experienced transient breath-holding episodes with generalized muscle stiffness and facial pallor while crying. At 11 months of age, 30-second-long episodes of apnea arose with

* Corresponding author at: Shikatacho 2-5-1 Department of Child Neurology, Okayama University Graduate School of Medicine, Dentistry, and Pharmaceutical Sciences, Okayama 700–8558 Japan. Tel.: +81 86 235 7372; fax: +81 86 235 7377.
E-mail address: magenta@md.okayama-u.ac.jp (H. Yoshinaga).

0022-510X/$ – see front matter © 2012 Elsevier B.V. All rights reserved.
doi:10.1016/j.jns.2011.12.015

Please cite this article as: Yoshinaga H, et al, A novel mutation in SCN4A causes severe myotonia and school-age-onset paralytic episodes, J Neurol Sci (2012), doi:10.1016/j.jns.2011.12.015

generalized hypertonia; these episodes were so severe that epileptic seizures were once suspected, but ictal EEG recordings did not indicate that this was the case. These episodes spontaneously disappeared, but at the age of two, the patient started to present daily fluctuating myotonia. The patient presented with a mask-like face with blepharospasm, grip myotonia, and dysarthria. These episodic myotonic attacks persisted for several minutes, hours, or even days, with fluctuation and created difficulties in standing, walking and upper-limb mobility. The symptoms seemed to be aggravated by cold (and were relieved during febrile illness) and fatigue, but not by potassium intake or exercise. The CK value fluctuated between 200 and 1000+ and tended to be high during myotonic attacks.

Fig. 1 depicts a generalized inter-episode feature when he was 5 years and 8 months old. Parental consent to present the photograph in Fig. 1 was obtained. He was of Herculean stature and exhibited several characteristic features, such as low-set ears, epicanthic folds, upturned nose, a long philtrum, puckered lips, short neck, hypertropic thighs, atrophic shoulder girdle muscles, pigeon breast, and joint contracture of the elbow. Accordingly, he was initially suspected as having a myogenic type of Schwarz–Jampel syndrome [4,11]. However, immunofluorescence stain for perlecan was normal in biopsied muscle and the histology revealed a nonspecific myopathic change with increased fiber variability. Acetazolamide, mexiletine, and phenytoin had some effect on his myotonic attacks. When these medications were discontinued on the day he underwent generalized anesthesia for the muscle biopsy, he experienced a very severe myotonic attack that involved the respiratory muscle.

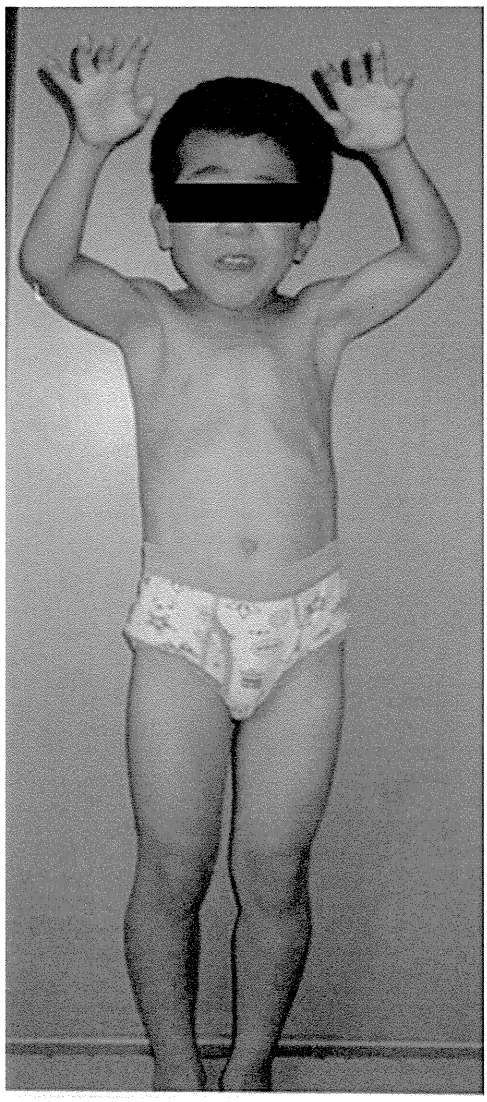

Fig. 1. The patient at 5 years and 8 months of age. Note his Herculean stature and hypertrophic thighs.

After 7 years and 8 months of age, paralytic episodes appeared that occurred several times a year thereafter, even in hot summertime temperatures. He complained of muscle weakness lasting from hours to several days at a time. His mother observed that his thighs become unusually soft during episodes. Neither exercise nor cooling brought about his episodic weakness.

2.2. Clinical electrophysiological analysis

Needle electromyography revealed diffuse continuous myotonic discharges accentuated by needle displacement with dive bomber sounds. Analysis of the compound muscle action potential (CMAP) amplitude before and after short or long exercise revealed no significant change [12]. Muscle cooling did not affect the CMAP either [13].

2.3. DNA analysis

Since there was no expansion of the repeat length at the DM1 locus with Southern blot, we analyzed the nucleotide sequence of *SCN4A* and *CLCN1* genes. Written informed consent was obtained from the parents for the mutation screening. This study was approved by the ethics committee of Kagoshima University Graduate School of Medical and Dental Sciences. Nucleotide sequence analysis of the patient's DNA showed a transition of A to C at the nucleotide in position 2077 (c.2077A>C) in *SCN4A* resulting in the substitution of isoleucine to leucine at amino acid in position 693 (p.I693L) (Fig. 2A). This mutation was not found in the DNA of the parents, both of whom were clinically non-affected. No mutations of *CLCN1* genes were identified by sequencing analysis.

Furthermore, the possibility of Schwarz–Jampel syndrome was excluded by re-sequencing all the exons and the flanking intronic regions of *HSPG2*. We enriched exonic fragments using the SureSelect Human All Exon v2 kit (Agilent, CA, USA), and read 50-bp fragments with the ABI SOLiD 4 sequencer (Applied Biosystems, CA, USA). We mapped 56,007,335 tags (89% of total tags) to human genome GRCh37.3/hg19 with BioScope 1.3.1 (Applied Biosystems), and read 2338 Mbp. Detection of SNVs with Avadis NGS (Strand Life Sciences, Bangalore, India) using default parameters revealed three homozygous missense SNPs that were all registered in dbSNP134 without any reference to clinical relevance (W71S, rs2254357, global minor allelic frequency (GMAF) = 0.475; G242V, rs2254358, GMAF = 0.476; and N765S, rs989994, GMAF = 0.068).

2.4. Sodium channel functional study

We cultured human embryonic kidney (HEK) cells and transfected them with wild-type or mutant human sodium channel constructs as previously described [14]. Na + currents were recorded by the conventional whole-cell patch clamp technique. As shown in Fig. 3A, the mutant channels were consistently activated at more hyperpolarized voltages than the wild-type channels. To further investigate this phenomenon, the normalized sodium conductance at each measured peak current was calculated and plotted against the corresponding voltage. There was a marked shift towards hyperpolarized voltages in the activation curve of p.I693L mutant channels indicating an enhancement of the activation (Fig. 3B. Table 1).

Please cite this article as: Yoshinaga H, et al, A novel mutation in SCN4A causes severe myotonia and school-age-onset paralytic episodes, J Neurol Sci (2012), doi:10.1016/j.jns.2011.12.015

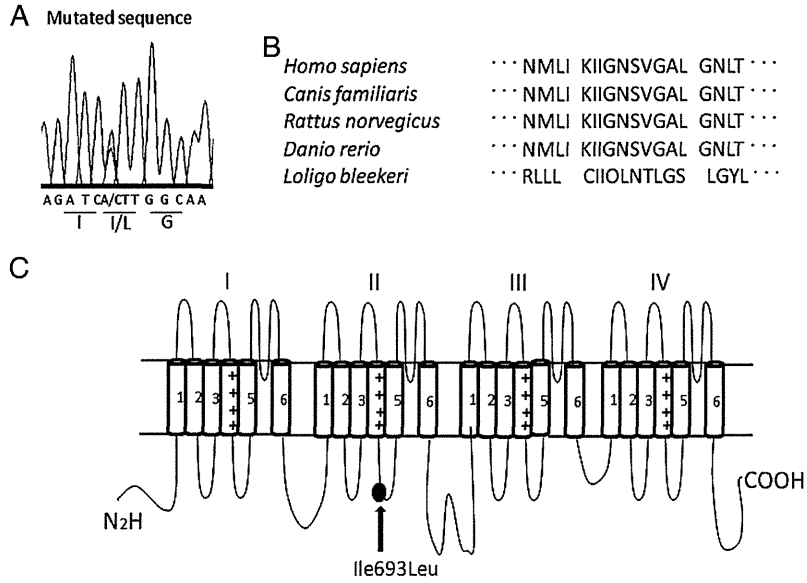

Fig. 2. A: DNA sequencing of the mutant region shows the transition of A to C at the nucleotide in position 2077 resulting in the substitution isoleucine (I) to leucine (L) at aminoacid in position 693 (I693L).B: Isoleucine residue in position 693 in Nav1.4 channel is preserved among homologs in many species.C: Schematic of the α subunit of Nav1.4 channel showing the six transmembrane segments (1–6) of each of the four domains (I–IV) and the location of p.I693L mutation (gray point).

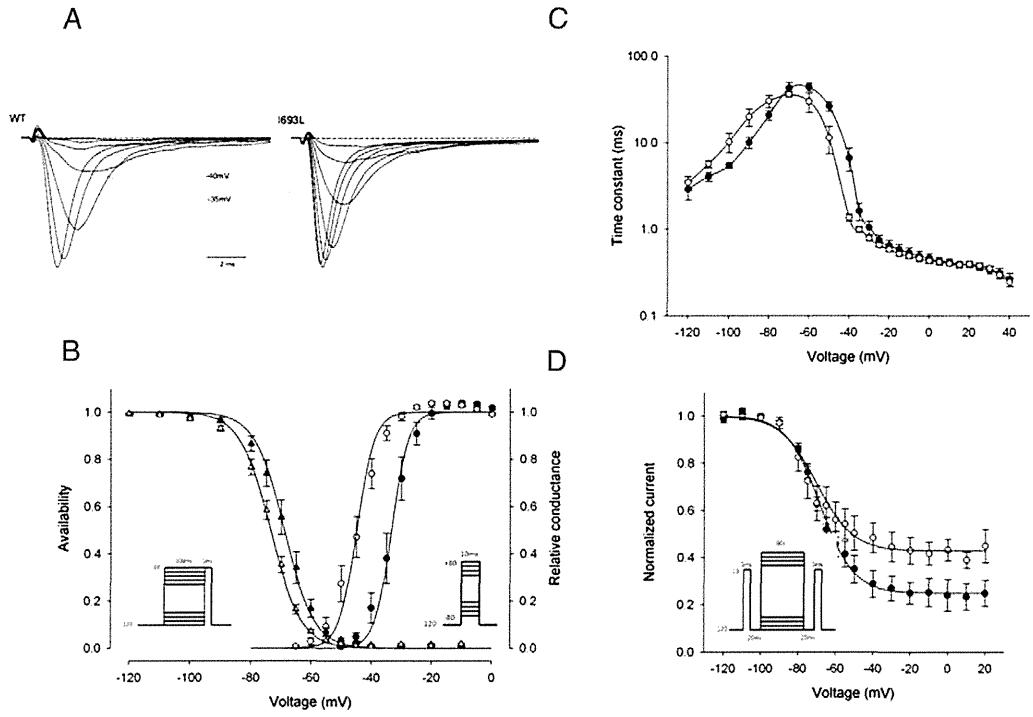

Fig. 3. A: Representative normalized currents recorded from HEK cells transfected with wild-type (WT) and I693L mutant channel and elicited by a series of 10 ms step pulse depolarizations from a holding potential of −120 mV to +40 mV in 5 mV increments. Activation is enhanced in I693L mutant channels.B: Activation (right-hand curves) for the wild-type ○ and I693L ● channels measured as the relative conductance of the peak sodium current elicited by depolarizing pulse from a holding potential of −120 mV to +40 mV (protocol in right inset). The activation voltage dependence of I693L mutant was shifted in the direction of hyperpolarization ($p<0.001$). Steady state fast inactivation (left-hand curves) for the wild-type △ and p.I693L ▲ channels measured as the relative peak current elicited by a −10 mV pulse after a 300 ms conditioning (protocol in left inset). We observed a shift towards negative voltages of the mutant constructs ($p=0.009$).C: Voltage dependence of the fast inactivation kinetics for the wild-type ○ and I693L ● channels measured by combining the data from three protocols (see results): a two-pulse recovery protocol (−120 mV to −80 mV), a two-pulse entry protocol (−70 mV to −40 mV) and a single-pulse relaxation protocol (−35 mV to +40 mV). The time constant for I693L channels was slightly slower at the negative voltages measured with the recovery protocol (n.s. $p>0.05$) and faster at the intermediate voltages measured with the entry protocol (from −50 mV to −35 mV $p<0.05$) than the wild-type. No difference was observed at more depolarized voltage.D: Peak sodium current elicited by a −10 mV test pulse was measured after a 60 s conditioning followed by a 20 ms gap at −120 mV to allow recovery from fast inactivation (protocol in the inset). The maximum extent of slow inactivation (1–I0) was smaller for I693L channels ●, revealing its impairment in comparison with the wild-type ○.

Please cite this article as: Yoshinaga H, et al, A novel mutation in SCN4A causes severe myotonia and school-age-onset paralytic episodes, J Neurol Sci (2012), doi:10.1016/j.jns.2011.12.015

Table 1
Gating parameter for WT and mutant Nav 1.4.

	Activation		Fast inactivation		Slow inactivation		
	V1/2(mV)	*k* (mV)	V1/2(mV)	*k* (mV)	V1/2(mV)	*k* (mV)	I0
WT	−33.3 ± 1.5 (9)	2.8 ± 0.4	−68.9 ± 1.6 (9)	5.0 ± 0.2	−68.3 ± 1.4 (5)	8.9 ± 1.1	0.25 ± 0.0522
p.I693L	−44.9 ± 1.5** (16)	2.9 ± 0.2	−73.5 ± 0.9* (5)	5.1 ± 0.2	−70.1 ± 3.3 (6)	9.6 ± 1.6	0.43 ± 0.0446*

Values are means + S.E.M, with number of experiments in parenthesis * significantly different from WT. $P<0.05$.
**significantly different from WT. $P<0.001$.

3. Discussion

Prior to identification of the sodium channel mutation, this patient was initially diagnosed as having a myogenic type of Schwartz–Jampel syndrome because of his characteristic appearance with severe myotonia [1,11]. The confusion between Schwartz–Jampel syndrome and sodium channelopathy was previously reported in a patient with myotonia permanence caused by G1306E mutation of SCN4A [4]. Our patient may also correspond to myotonia permanence, and he exhibited severe myotonic symptoms as apneic episodes from the neonatal period. Several patients with a *SCN4A* mutation, who showed severe symptoms including respiratory distress from an early neonatal period have also been reported [7,8]. One of these cases resembled Schwartz–Jampel syndrome [8].

Our patient showed severe myotonic episodes in his early infancy and then subsequent paralytic episodes. This case provides an example of the complexity and overlap of the clinical features of the sodium channel myotonic disorders, which sometimes make their classification difficult.

Some medications, including local anesthetics, anticonvulsants, and antiarrhythmics such as mexiletine, have shown efficacy for myotonic sodium channelopathies by blocking the sodium channel [2,15]. A carbonic anhydrase inhibitor, acetazolamide, is known to prevent paralytic attack but its antimyotonic action is in question. The myotonia of our patient showed a good response to mexiletine, phenytoin and acetazolamide, although carmabazepin showed little effect. Further studies are needed to understand the difference in efficacy between these drugs and the effects of acetazolamide.

The recently proposed standardized protocols involving short and long exercise tests in electromyographic analysis have improved the diagnosis of the subgroup of mutations in muscle channelopathies [12,13]. Fournier et al. [13] reported that combining the responses to several tests defined five electromyographic patterns that correspond to the subgroups of mutations. We applied their protocol to our patient and defined the response as pattern III [11] in which excitability is not impeded by any of the exercise trials. In their report [11], patients carrying G1306A or I693T (same locus on Nav 1.4 as ours [16]) sodium channel mutation also exhibited pattern III.

Functional analysis of the mutant channel revealed that the activation of the mutant channel was markedly enhanced in concordance with the enhanced excitability of our patient. However hyperpolarized shift of the steady-state inactivation curve which should reduce excitability, was also in a milder way observed in the mutant channel. The former may prevail over the latter, explaining the enhanced excitability which contributes to myotonia. Other mutations such as V445M [17], L689I [18], I704M, including the aforementioned I693T [16], have been found to similarly enhance both activation and fast inactivation and are often associated with myotonia.

Also, our data showed disrupted slow inactivation in the mutant construct, a defect which is expected to predispose to prolonged attack of paralysis. Our patient started to show episodic weakness recently. Again, I693T mutation showed an enhancement of activation with a slight shift towards hyperpolarized voltages for the steady state inactivation as well as a severely impaired slow inactivation [16]. The channel gating defects for I693T and its electromyographic pattern are strikingly similar with those observed for I693L. Unexpectedly, the I693T patient suffered from cold-induced weakness with a very mild myotonia [16]. The difference in hydrophobicity between the two mutated amino acids or the underlining genetic or environmental factors such as drug treatment can possibly modulate the expression of the disease.

Two other mutations, L689I and T70M, have been reported in the intracellular loop linking segments 4–5 of domain II in *SCN4A* [18]. Both have a phenotype of hyperkalemic periodic paralysis with a predominant weakness. The functional analysis of these mutant channels again revealed an enhancement of activation, and an impaired slow inactivation to a similar extent as for I693L mutant. These data and ours confirm the fact that the IIS4-S5 linker is one of the determinant regions for the sodium channel slow inactivation and to a various extent for the activation.

4. Conclusion

Further study of the genotype–phenotype correlations through individual cases will increase our knowledge of the variability of signs in this group of diseases and may also provide us with deeper insight into the function of the various regions of sodium channel proteins.

Acknowledgement

We thank Dr. Steve Cannon, University of Texas, for providing the expression vectors. This study was supported by Grants-in-Aids from the Ministry of Education, Culture, Sports, Science and Technology as well as the Ministry of Health, Labor and Welfare of Japan.

References

[1] Lehmann-Horn F, Rudel R, Jurkat-rott K. Nondystrophic myotonias and periodic paralyses. In: Engel AG, Franzini-Armstrong C, editors. Myology. 3rd ed. New York: McGraw Hill; 2004. p. 1257–300.
[2] Matthews E, Fialho D, Tan SV, Venamce SL, Cannon SC, Sternberg D, et al. The non-dystrophic myotonicas: molecular pathogenesis, diagnosis and treatment. Brain 2010;133:9–12.
[3] Plassart E, Eymard B, Maurs L, Hauw JJ, Lyon-Caen O, Fardeau M. Paramyotonia congenita: genotype to phenotype correlations in two families and report of a new mutation in the sodium channel gene. J Neurol Sci 1996;142:126–33.
[4] Colding-Jorgensen E, Duno M, Vissing J. Autosomal dominant monosymptomatic myotonia premanens. Neurology 2006;67:153–5.
[5] Lerche BH, Heine R, Pika U, George Jr AL, Mitovic N, Browatzki M, et al. Human sodium channel myotonia: slowed channel inactivation due to substitutions for a glycine within the III-IV linker. J Physiol 1993;470:13–22.
[6] Rudel R, Ricker K, Lehmann-Horn F. Genotype–phenotype correlations in human skeletal muscle sodium channel diseases. Arch Neurol 1993;50:1241–8.
[7] Lion-Francois L, Mignot C, Vicart S, Manel V, Sternberg D, Landrieu P, et al. Severe neonatal episodic laryngospasm due to de novo SCN4A mutation. Neurology 2010;75:641–5.
[8] Gay S, Dupuis D, Faovre L, Masurel-Paulet A, Labenne M, Colombani M, et al. Severe neonatal non-dystrophic myotonia secondary to a novel mutation of the voltage-gated sodium channel (SCN4A) gene. Am J Med Genet A 2008;146:380–3.
[9] Goldin AL. Mechanisms of sodium channel inactivation. Curr Opin Neurobiol 2003;13(3):284–90.
[10] Hayward LJ, Sandoval GM, Cannnon SC. Defective slow inactivation of sodium channels contributes to familial periodic paralysis. Neurology 1999;52:1447–53.

Please cite this article as: Yoshinaga H, et al, A novel mutation in SCN4A causes severe myotonia and school-age-onset paralytic episodes, J Neurol Sci (2012), doi:10.1016/j.jns.2011.12.015

[11] Topaloglu BH, Serdaroglu A, Okan M, Gucuyener K, Tope M. Improvement of myotonia with carbamazepine in three cases with the Schwartz–Jampel syndrome. Neuropediatrics 1993;24:232–4.
[12] Fournier E, Arzel M, Sternberg D, Vicart S, Laforet P, Eymard B, et al. Electromyography guides toward subgroups of mutations in muscle channelopathies. Ann Neurol 2004;56:650–61.
[13] Fournier E, Viala K, Gervais H, Sternberg D, Arzel M, Vicart S, et al. Cold extends electromyography distinction between ion channel mutations causing myotonia. Ann Neurol 2006;60:356–65.
[14] Hayward LJ, Brown Jr RH, Cannon SC. Inactivation defects caused by myotonia-associated mutations in the sodium channel III–IV linker. J Gen Physiol 1996;107:559–76.
[15] Heatwole CR, Moxley III RT. The nondystrophic myotonia. Neurotherapeutics 2007;4:238–51.
[16] Plassart-Schiess E, Lhuillier L, George Jr AL, Fontaine B, Tabti N. Functional expression of the Ile693Thr Na+ channel mutation associated with paramyotonia congenital in a human cell line. J Physiol 1998;507(3):721–7.
[17] Takahashi MP, Cannon SC. Enhanced slow inactivation by V 445M: a sodium channel mutation associated with myotonia. Biophys J 1999;76:861–8.
[18] Bendahhou S, Cummins TR, Kula RW, Fu YH, Ptacek LJ. Impairment of slow inactivation as a common mechanism for periodic paralysis in DIIS4-S5. Neurology 2002;58:1266–72.

Please cite this article as: Yoshinaga H, et al, A novel mutation in SCN4A causes severe myotonia and school-age-onset paralytic episodes, J Neurol Sci (2012), doi:10.1016/j.jns.2011.12.015

RESEARCH ARTICLE

Human Mutation

OFFICIAL JOURNAL
HGVS
HUMAN GENOME VARIATION SOCIETY
www.hgvs.org

Mutations in the C-Terminal Domain of ColQ in Endplate Acetylcholinesterase Deficiency Compromise ColQ–MuSK Interaction

Tomohiko Nakata,[1,2] Mikako Ito,[1] Yoshiteru Azuma,[1,2] Kenji Otsuka,[1] Yoichiro Noguchi,[1] Hirofumi Komaki,[3] Akihisa Okumura,[4] Kazuhiro Shiraishi,[5] Akio Masuda,[1] Jun Natsume,[2] Seiji Kojima,[2] and Kinji Ohno[1]*

[1]*Division of Neurogenetics Center for Neurological Diseases and Cancer, Nagoya University Graduate School of Medicine, Nagoya, Japan;* [2]*Department of Pediatrics Nagoya University Graduate School of Medicine, Nagoya, Japan;* [3]*Department of Child Neurology National Center Hospital, National Center of Neurology and Psychiatry (NCNP), Tokyo, Japan;* [4]*Department of Pediatrics Juntendo University Faculty of Medicine, Tokyo, Japan;* [5]*Department of Pediatrics Utano National Hospital, Kyoto, Japan*

Communicated by Lars Bertram

Received 19 January 2013; accepted revised manuscript 19 March 2013.
Published online 29 March 2013 in Wiley Online Library (www.wiley.com/humanmutation). DOI: 10.1002/humu.22325

ABSTRACT: Acetylcholinesterase (AChE) at the neuromuscular junction (NMJ) is mostly composed of an asymmetric form in which three tetramers of catalytic AChE subunits are linked to a triple helical collagen Q (ColQ). Mutations in *COLQ* cause endplate AChE deficiency. We report three patients with endplate AChE deficiency with five recessive *COLQ* mutations. Sedimentation profiles showed that p.Val322Asp and p.Arg227X, but not p.Cys444Tyr, p.Asp447His, or p.Arg452Cys, inhibit formation of triple helical ColQ. In vitro overlay of mutant ColQ-tailed AChE on muscle sections of *Colq*$^{-/-}$ mice revealed that p.Cys444Tyr, p.Asp447His, and p.Arg452Cys in the C-terminal domain (CTD) abrogate anchoring ColQ-tailed AChE to the NMJ. In vitro plate-binding assay similarly demonstrated that the three mutants inhibit binding of ColQ-tailed AChE to MuSK. We also confirmed the pathogenicity of p.Asp447His by treating *Colq*$^{-/-}$ mice with adeno-associated virus serotype 8 carrying mutant *COLQ*-p.Asp447His. The treated mice showed no improvement in motor functions and no anchoring of ColQ-tailed AChE at the NMJ. Electroporation of mutant *COLQ* harboring p.Cys444Tyr, p.Asp447His, and p.Arg452Cys into anterior tibial muscles of *Colq*$^{-/-}$ mice similarly failed to anchor ColQ-tailed AChE at the NMJ. We proved that the missense mutations in ColQ–CTD cause endplate AChE deficiency by compromising ColQ–MuSK interaction at the NMJ.
Hum Mutat 34:997–1004, 2013. © 2013 Wiley Periodicals, Inc.

KEY WORDS: COLQ; collagen Q; neuromuscular; acetylcholinesterase; myasthenic syndromes

Introduction

Congenital myasthenic syndromes (CMS) are clinically and genetically heterogeneous inherited disorders characterized by neuromuscular transmission defect caused by mutations affecting proteins expressed at the neuromuscular junction (NMJ) [Engel et al., 2003]. The synaptic type of CMS is caused by the absence of the asymmetric form of acetylcholinesterase (AChE) from the endplate [Engel et al., 1977]. Endplate AChE deficiency is characterized by generalized muscle weakness, fatigue, scoliosis, minor facial abnormalities, and episodes of respiratory distress [Mihaylova et al., 2008]. In the absence of AChE, the duration of the endplate currents are prolonged, so that it outlasts the refractory period of the skeletal muscle sodium channel, which in turn evokes repetitive compound muscle action potentials (CMAPs). Four mechanisms lead to defective neuromuscular signal transmission in endplate AChE deficiency [Engel et al., 1977; Ohno et al., 1998]. First, the prolonged endplate currents lead to overload of Ca^{2+} ions at the postsynaptic sarcoplasm, which causes endplate myopathy with loss of acetylcholine receptor (AChR). Second, excessive ACh at the synaptic space causes desensitization of AChR. Third, repeated opening of AChR causes staircase summation of endplate potentials, which depolarizes the resting membrane potential and makes the muscle sodium channel irresponsive to an endplate potential. Fourth, lack of ColQ at the NMJ diminishes the amount of membrane-bound MuSK and reduces phosphorylation of the AChR β subunit, which compromises AChR clustering [Sigoillot et al., 2010]. Lack of effects of cholinesterase inhibitors, or even worsening of the symptoms with them, in patients with endplate AChE deficiency suggests that lack of AChE rather than lack of AChR is a key underlying mechanism leading to myasthenic symptoms.

Endplate AChE deficiency is not caused by mutations in the *ACHE* gene (NM_000665.3; MIM #100740) encoding the catalytic subunit but is caused by recessive mutations in the *COLQ* gene (NM_005677.3; MIM #603033) encoding the collagenic tail subunit [Ohno et al., 1998]. There are two major types of AChE in the skeletal muscle: (1) globular forms consisting of monomers (G_1), dimmers (G_2), or tetramers (G_4) of the T isoform of the catalytic subunit ($AChE_T$, NP_000656.1), and (2) asymmetric forms consisting of one, two, or three homotetramers (A_4, A_8 and A_{12}, respectively) of $AChE_T$ attached to a triple-stranded collagenic tail (ColQ) [Massoulie, 2002], which are hereafter called ColQ-tailed

Additional Supporting Information may be found in the online version of this article.

*Correspondence to: Kinji Ohno, Division of Neurogenetics, Center for Neurological Disease and Cancer, Nagoya University Graduate School of Medicine, 65 Tsurumai, Showa-ku, Nagoya 466-8550, Japan. E-mail: ohnok@med.nagoya-u.ac.jp

Contract grant sponsors: Ministry of Education, Culture, Sports, Science, and Technology of Japan, and the Ministry of Health, Labor, and Welfare of Japan.